NTNU

Norwegian University of
Science and Technology

Theoretical study and mathematical modelling on the reaction rates in the SiMn-production process

Håkon Aleksander H Olsen

Materials Science and Engineering
Submission date: July 2016
Supervisor: Merete Tangstad, IMTE

Norwegian University of Science and Technology
Department of Materials Science and Engineering

Spring 2016

A theoretical study on the reaction rates in the SiMn-production process

Håkon Aleksander Hartvedt Olsen

Materials Technology
Submission date: july 2016
Supervisor: Professor Merete Tangstad

Department of Materials Science and Engineering
Norwegian University of Science and Technology

Preface

This thesis describes the investigation of the silicomanganese production process through the use of a computational model. It is the main project and evaluation basis for the course TMT4905 Materials Technology, Master's Thesis at the Norwegian University of Science and Technology. The work was performed during the spring semester of 2016, and was supervised by Professor Merete Tangstad at the Department of Materials Science and Engineering.

This work is founded by the the research senter SFi Metal Production. The work is part of the Research Domain 2, Primary Metal Production, with Professor Merete Tangstad as leader.

Trondheim, July 2016

Håkon Olsen

Acknowledgements

For the opportunity to do this work as well as helping me through this work and supervising it all, the first and most of my thanks goes to Merete Tangstad. For all the discussions, lectures and guidance she's given me over the course of this project, I am very grateful.

Secondly I want to thank Kai Tang, Joakim Holtan and Pyonghwa Kim for providing me with much needed data.

Thirdly, I want to thank my classmates and the SiManTi-group for providing additional opportunities for discussion as well as the occasional tips and tricks to help me along the way.

Lastly I want to thank my girlfriend Olava for all her help and support, especially when things were going slowly and the motivation was at rock bottom.

Abstract

The reduction rate of MnO and SiO_2 in the furnace stage of metallurgical silicomanganese production has been studied to increase the current understanding of the SiMn-alloy production process. Using thermodynamic data and experimental values, a computational model has been constructed in MATLAB R2016B, based on the general relations for the reaction rates of the most prominent reactions found in the process. Furthermore, general formulas for the activities of MnO, SiO_2, Mn and Si, as well as the carbon saturation in the metal, were created based of data from FACTSAGE.

The formulas for activities and carbon saturation were found to be able to replicate the values from FACTSAGE to a very high degree for the concentrations found during the silicomanganese production process.

The model was found to be able to replicate most of the experiments to a very high degree, producing slag and metal concentrations that were within a tens of a percent of the experimental value through the application of our knowledge of the thermodynamics and kinetics of the system.

From the comparison of three experiments with Assmang ore and three with Comilog ore, Assmang ore was found to reduce faster and at a lower temperature compared to Comilog ore.

The foaming phenomena was studied and the rate of reaction was found to increase several fold during the foaming. This was believed to be due to an increased reaction area between the carbon in the crucible wall and the coke, and the slag.

HeFeMn was found to reduce the temperature at which Assmang ore and quartz starts reducing with abour 75 °C.

Abstract in norwegian

Reduksjonsraten til MnO og SiO_2 i den nedre delen av ovnen i metallurgisk silikomanganproduksjon har blitt studert for å øke vår forståelsen av produksjonsprosessen til SiMn-legeringer. Ved bruk av termodynamiske og experimentelle verdier, har en matematisk modell blitt konstruert i MATLAB R2016B basert på de generelle relasjonene til reactionsratene til de mest fremtredende reactionene i prosessen. Videre har generelle formler for aktivitetene til MnO, SiO_2, Mn and Si, i tillegg til løsligheten til karbon i metallet blitt laget basert på verdier fra FACTSAGE

Formlene for aktiviteter og karbonløselighet klarte replikere verdiene fra FACTSAGE til veldig høy grad for konsentrasjonen funnet under produksjonen av silikomangan.

Modellen ble funnet å være kapabel til å replikere mesteparten av eksperimentene til en høy grad, og den produserte slag- og metallkonsentrasjoner som var innenfor en tiendels prosent av de eksperimentelle verdiene gjennom bruken av vår kunnskap om termodynamikk og kinetikk for systemet.

Fra en sammenligning mellom tre eksperimenter med Assmang malm og tre med Comilog malm, ble Assmang malm vist å reduseres raskere og ved lavere temperaturer enn Comilog malm.

Boblefenomenet ble studert og reaksjonsraten ble funnet til å øke sterkt under bobling. Dette er trodd at kommer av en økt reaksjonsområde mellom karbon i veggene og koksen, og slaggen.

Det ble funnet at HCFeMn reduserer temperatures som trengs for reduksjon av Assmang malm med omtrendt 75 °C.

Contents

1. Introduction

This chapter contains an introduction of the commercial production route used to produce SiMn alloys, and how computer models are utilized in the SiMn industry today. Lastly the goal of this thesis project will be discussed together with the assumptions and limitations for the project. Some term are defined here to provide clarity for the following sections [1]:

Charge: The mixture of raw materials inserted at the top of the furnace.
Coke bed: The part of the furnace where the ore is melted in a surplus of carbon.
Flux: A material added to the charge for changing slag properties, e.g. basicity and activities.
Pre-reduction zone: The section of the furnace where the flux and ore are primarily solid. This is above the coke bed.
Slag: Oxide mixture where the manganese is present as MnO.

1.1. Silicomanganese

Silicomanganese is an alloy composed primarily of Mn and Si. Typical compositions lie between 60-70 wt% Mn, 0.1-2 wt% C, and 17-30 wt% Si, with the remainder consisting of Fe and other impurities [2]. The production of silicomanganese is performed by carbothermic reduction of high MnO slags from FeMn-production, manganese ore, quartz, dolomite and coke in an electric arc furnace. The metal producing reactions can be summed up to as shown in equation 1 and 2.

$$MnO_x + C = Mn + CO/CO_2 \tag{1}$$

$$SiO_2 + C = Si + CO \tag{2}$$

Silicomanganese is primarily used as a source of alloying elements in steel production as an alternative to high carbon ferromanganese and ferrosilicon. Historically a mixture of HC-FeMn, high carbon ferromanganese, and FeSi, ferrosilicon, was used as a source of alloying elements, but a trend towards using SiMn instead has been observed in more recent times [2].

In 2011 the world wide production of SiMn amounted to 11.8 million tons. Norway is currently one of the largest exporters of SiMn, ranking fourth behind India, Ukraine and South Africa. The global market for SiMn is heavily tied to the steel market, due to the steel industry being the primary consumer of SiMn [3].

Standard silicomanganese is produced from a mixture of HCFeMn slag, manganese ores, quartzite, (Fe)Si-remelts or off grade qualities, and coke. The manganese ore comes from a limited number of workable deposits, most of which lie in Asia and Africa, and with a single field constituting for more than 70% of the world's total land-based reserves[2]. Quartzite is more common and readily accessible from various mines, while the coke is converted from common coal through heating in absence of air [2]. Slag elements suck as CaO, Al_2O_3 and MgO are added through and fluxes like dolomite and limestone.

Typically 500-1000 kg of ferromanganese slag, containing 35 to 45 weight percent manganese oxide and 15-30 weight percent silica, is formed during the production of one ton of HCFeMn alloy. Because of the high cost of manganese ores, this slag is often used as a source of manganese in silicomanganese production. By utilizing ferromanganese slag in silicomanganese production, a very high total yield of manganese can be achieved; it does, however, increase the energy consumption of the process [4]. Due to the low melting temperature of FeMn slag, it is not used as the main source for MnO as this leads to a lower process temperature.

Silicomanganese is produced from carbothermic reduction of oxide raw materials in electric submerged arc furnaces (SAF), which is also used for SiMn and FeMn alloys. A process temperature of around 1600 to 1650°C is necessary to obtain sufficiently high Si content in the metal, as well as a low MnO content in the discard slag. Due to these high temperature requirements, operation of the SiMn process is often more difficult[5].

In the SAF, coke is used as the main reductant to form Fe, Si and Mn metal. The full process happens over the course of several steps and in different parts of the furnace. Carbon monoxide is formed in the lower regions of the furnace, which reduces the FeO as well as the higher manganese oxides higher up. Table 1 gives and example of average operating data for a 27 MW furnace producing standard silicomanganese alloy, while table 2 and figure 1 shows the material balance in the production process. Table 3 shows the metal and slag composition following the material balance in table 2.

Table 1: Average operating results for a plant producing standard silicomanganese alloy in a 27 MW submerged arc furnace [2]

Average furnace load	MW	27
Operating time	%	99
Power consumption	kWh/ton	3500
Production per day	ton/day	175
Production of slag	kg/ton SiMn	1225
Coke	kg/ton SiMn	360
Electrode consumption	kg/ton SiMn	30
Mn recovery in saleable metal	%	88

Table 2: Material balance for production of standard silicomanganese alloy in a 27 MW submerged arc furnace [2]

Materials	**Kg**	**Mn**	**Fe**	**Si**	**SiO_2**	**Al2O3**	**CaO**	**MgO**	**P**	**FixC**
Mn-ore	396	200	40		16	1	23	2	0.16	
HC-slag	1370	423			308	156	181	82		
Metal in slag	223	174	33							7
Quartz	411		3		399	14	7	7		
Coke I	216		1		7	5	1	0	0.11	160
Coke II	144		1		8	5			0.03	104
Dolomite	100					3	29	17		
Si-met, sculls	139		4	79	36	7	7			1
Products		**797**	**82**	**79**	**774**	**191**	**248**	**108**	**0.3**	**272**
SiMn-met	1000	705	81	192					0.5	15
SiMn-slag	1200	75			520	180	242	103		
Metal in slag	25	17	2	5					0.01	0.37

Table 3: Slag and metal compositions following the material balance in table 2

Metal composition (%)		**Slag composition (%)**	
Mn	70.5	MnO	8.1
Fe	8.1	SiO_2	43.3
Si	19.2	Al_2O_3	15.0
C	1.5	CaO	20.2
P	0.05	MgO	8.6

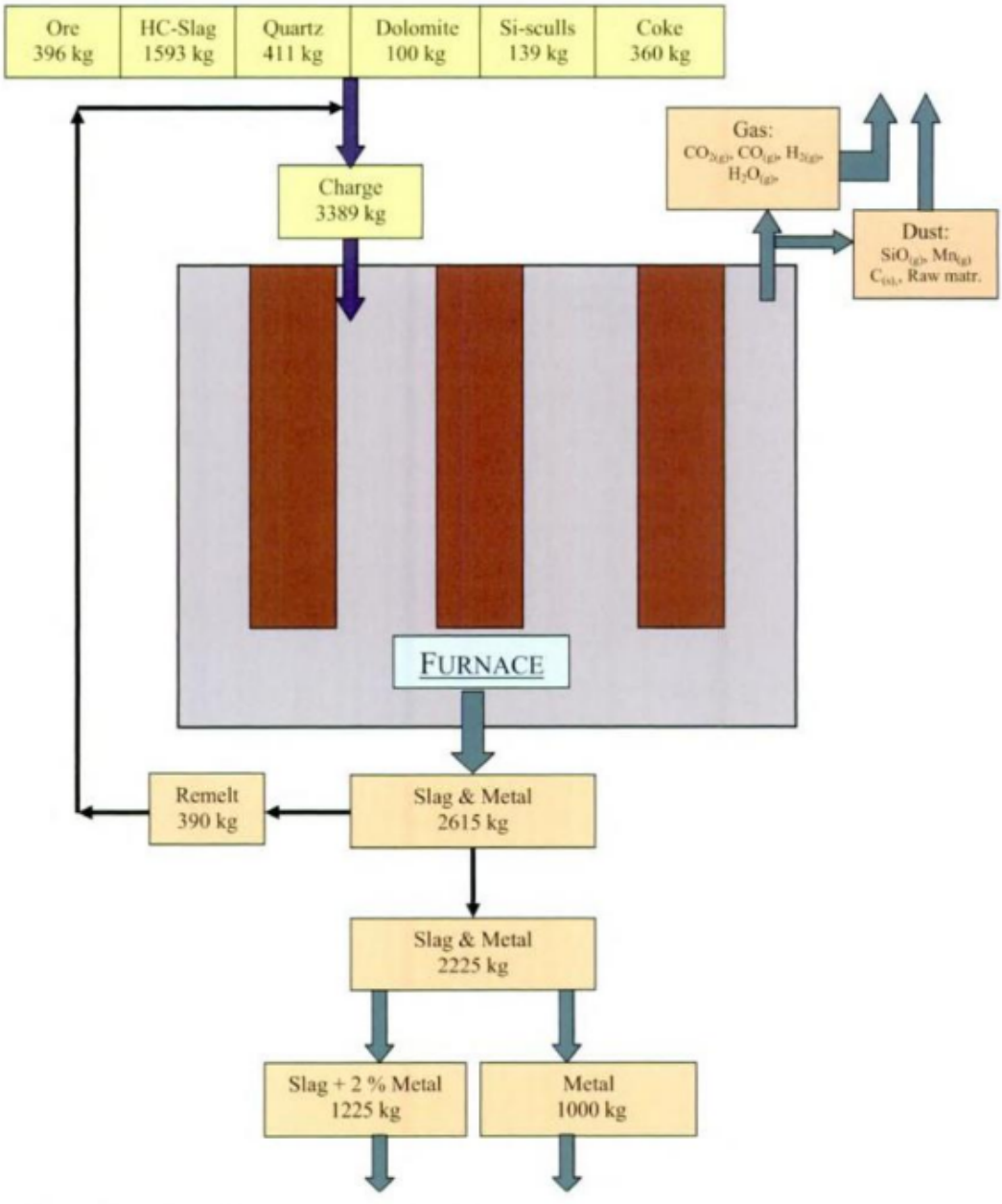

Figure 1: Mass flow for production of one ton standard silicomanganese alloy in a 27 MW submerged arc furnace [2]

During the silicomanganese process, carbon reacts with the oxides to form metal and carbon oxides. Although other reactions can occur, the only gases considered leaving the system in this work are CO_2

and CO. The amount of other gases such as SiO and Mn gas are considered to be negligible. The amount of impurities in the raw materials such as phosphorous, sulphur and nitrogen is also considered to be negligible.

The silicomanganese production process can be split into several steps found in different zones of the furnace. Figure 2 shows the different zones from a furnace excavation; the charge, the dry coke bed, the coke bed with slag, the pure slag, and the metal. Generally the pre-reduction happens in the higher and colder pre-reduction zone, which is the area above the slag, while the reduction of MnO and SiO_2 happens in the lower high-temperature zone, which is the area containing slag.

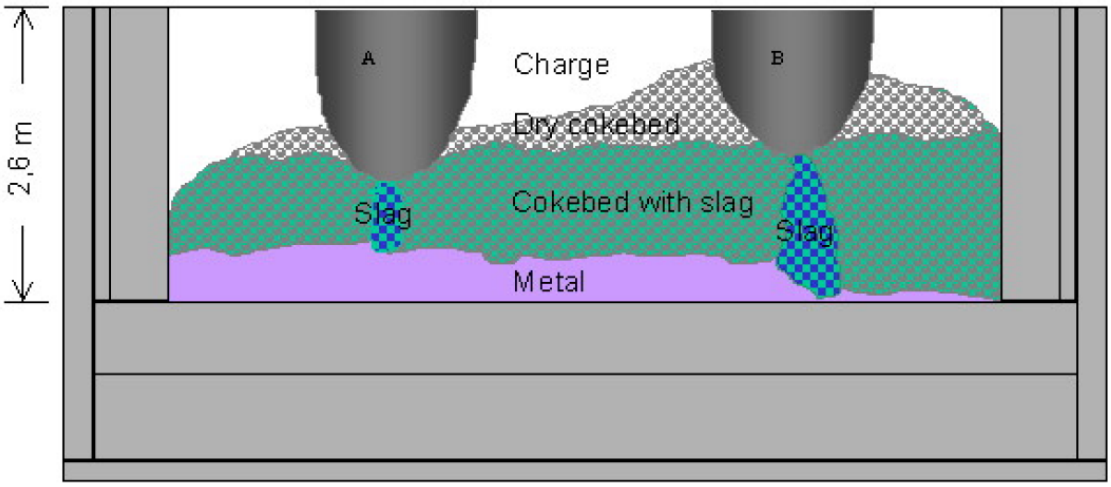

Figure 2: Zones described from an excavated industrial SiMn-furnace [5].

The pre-reduction step is considered to find place in the charge above the slag and coke bed. Here the iron oxide is reduced to metallic iron and the manganese oxides are reduced to MnO [4] following the reactions 3 and 4. In this area, any water is evaporated and any carbonates are thermally decomposed following the reactions 5 and 6.

$$FeO + CO \Rightarrow Fe + CO_2 \tag{3}$$

$$MnO_x + CO \Rightarrow MnO + CO_2 \tag{4}$$

$$H_2O(l) \Rightarrow H_2O(g) \tag{5}$$

$$MeO_x(CO_2)_y \Rightarrow MeO_x + yCO_2 \tag{6}$$

Here Me refers to any metal atom that binds carbonates in this way, most commonly Ca, Mg and Mn.

Melting of the slag as well as the first reduction of MnO happens around the top of the coke bed, where the temperature is expected to lie between 1523K and 1873K. Slag samples taken from this section of the furnace have been found to contain about 10wt% MnO [4]. The rate of MnO reduction is found to be

fast in the early stages when there still is solid MnO, before it decreases proportionally to the solid MnO content [3]. The reduction of manganese oxide is defined by equation 7.

$$MnO + C \Rightarrow Mn + CO \tag{7}$$

Finally silica gets reduced to silicon metal as the last step in the process, which happens around 1823K to 1923K. This reduction is considered to start around the point when the concentration of MnO drops below 10wt% [4]. The reduction of silicon dioxide is defined by equation 8.

$$SiO_2 + 2C \Rightarrow Si + 2CO \tag{8}$$

1.2. Project goals

The aim of this project is to produce a computational model which can simulate the process in the lower part of the silicomanganese furnace, and also to evaluate the model's validity. Furthermore, using this model, the goal is to gain improved understanding over the reaction mechanics involved in the production of silicomanganese. Through applying the model on data from several experimental setups, values for the reactivity of different ores will be investigated. The effect of different temperatures and additives on these values will be studied as well. Experimental data from Kim (2016) [6], Holtan (2016) [7], and Skjervheim (1994) [8] will be used to adjust and validate the model.

2. Theory

This chapter gives an overview of the underlying theoretical principles for the studied reactions. Included is previous work conducted on this field, as well as the general chemical principles applied. Data on both relevant thermodynamics and kinetics are presented, together with phase diagrams and descriptions of the slag and metal phase systems.

The two primary parts of the furnace, the pre-reduction part and the high-temperature zone, are both discussed here, but with a focus on the high-temperature zone. The many relations in this zone and how they affect the reaction rates will be presented.

2.1. Thermodynamics

In the pre-reduction zone, manganese and oxygen form several different oxides, and they all exist as stable crystalline phases[9]. Manganese ore predominantly contains higher manganese oxides such as MnO_2, Mn_2O_3, and Mn_3O_4, while MnO is typically only found in the slag[2]. During the pre-reduction phase, higher oxides are reduced by CO gas according to the equations 9 through 11 [10][11]. Figure 3 shows the stability diagram for the Mn-O system, and the reactions shown in equation 9 through 11 take place on the borderlines between the phases shown in the diagram.

$$MnO_2 + \frac{1}{2}CO = \frac{1}{2}Mn_2O_3 + \frac{1}{2}CO_2 \qquad (\Delta H^\circ_{298} = -99.9kJ) \tag{9}$$

$$\frac{1}{2}Mn_2O_3 + \frac{1}{6}CO = \frac{1}{3}Mn_3O_4 + \frac{1}{6}CO_2 \qquad (\Delta H^\circ_{298} = -31.3kJ) \tag{10}$$

$$\frac{1}{3}Mn_3O_4 + \frac{1}{3}CO = MnO + \frac{1}{3}CO_2 \qquad (\Delta H^\circ_{298} = 16.9kJ) \tag{11}$$

As the change in enthalpy is negative for the three reactions 9 - 11, these reactions provide heat to the system. This important when choosing raw materials, as using an ore with a higher oxygen to manganese ratio will reduce the energy consumption of the furnace. Although the main reductant is CO (g) as used in equation 9 through 11 [12], the highest oxides can decompose through temperature alone [9], while some of the Mn_3O_4 in some case isn't reduced by CO, but by the solid carbon in the cokebed.

These reactions characterize the pre-reduction zone, and are accompanied by the solid state reduction of FeO and the decomposition of carbonates as shown in chapter 1. The products of these reactions all end up in the high-temperature zone in the coke bed as a slag. In this part of the furnace, MnO and SiO_2 will be reduced with carbon, but the more stable oxides, CaO, MgO, and Al_2O_3 will remain in the slag phase.

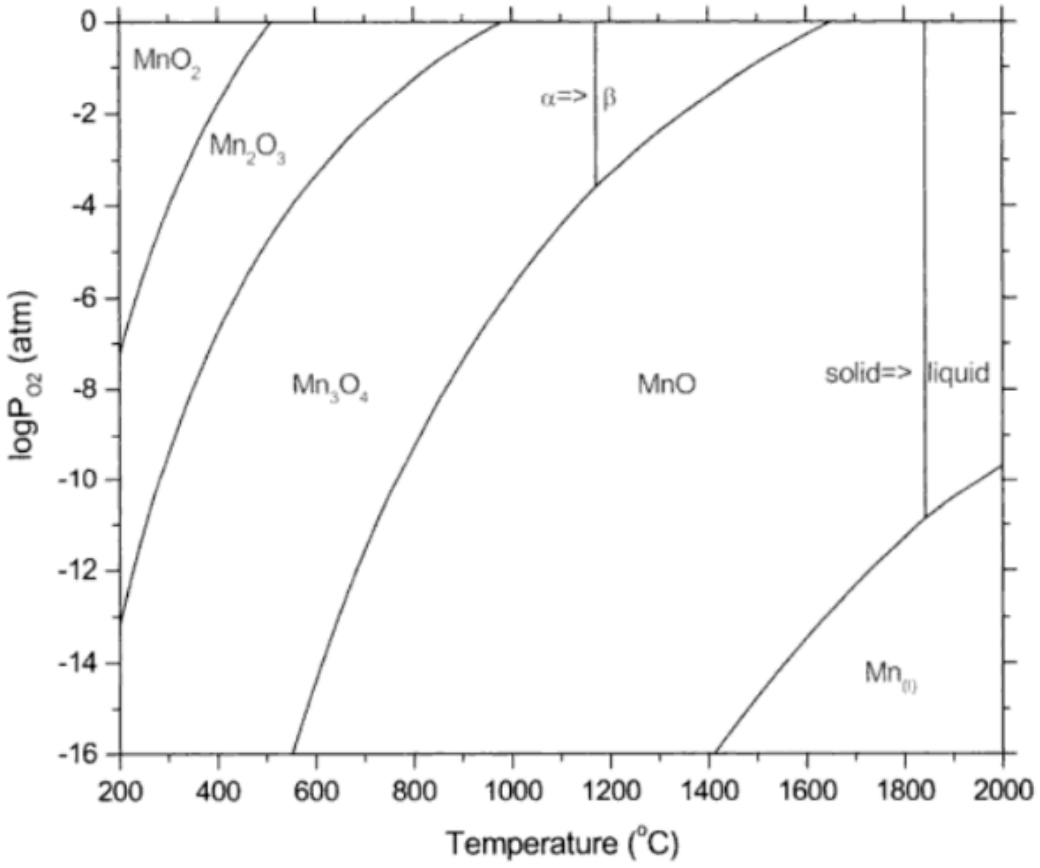

Figure 3: Stability diagram of Mn-O ststem as a function of temperature in °C and oxygen pressure in atm [2].

2.1.1. The slag system

The slag system in the silicomanganese production process is very complex, including up to five oxides, MnO, SiO_2, CaO, Al_2O_3, and MgO, after the iron has been reduced and without accounting for impurities. Figure 4 shows calculated phase and liquidus relations for one pair of acidic and basic slag relationships. The system's complexity leads to the need of severe simplification before attempts at modelling the system can be attempted. It can be seen from the figure however, that at temperatures above 1500°C the slag mixture is pure liquid for most slags with MnO-content below 45wt% and SiO_2 content above 30wt%. Assuming pure liquid for the system makes things easier, especially in regards to calculating activities. This assumption can be made for the metal phase as well, as the temperatures in the bottom of the furnace are generally much higher than the melting point of the metal.

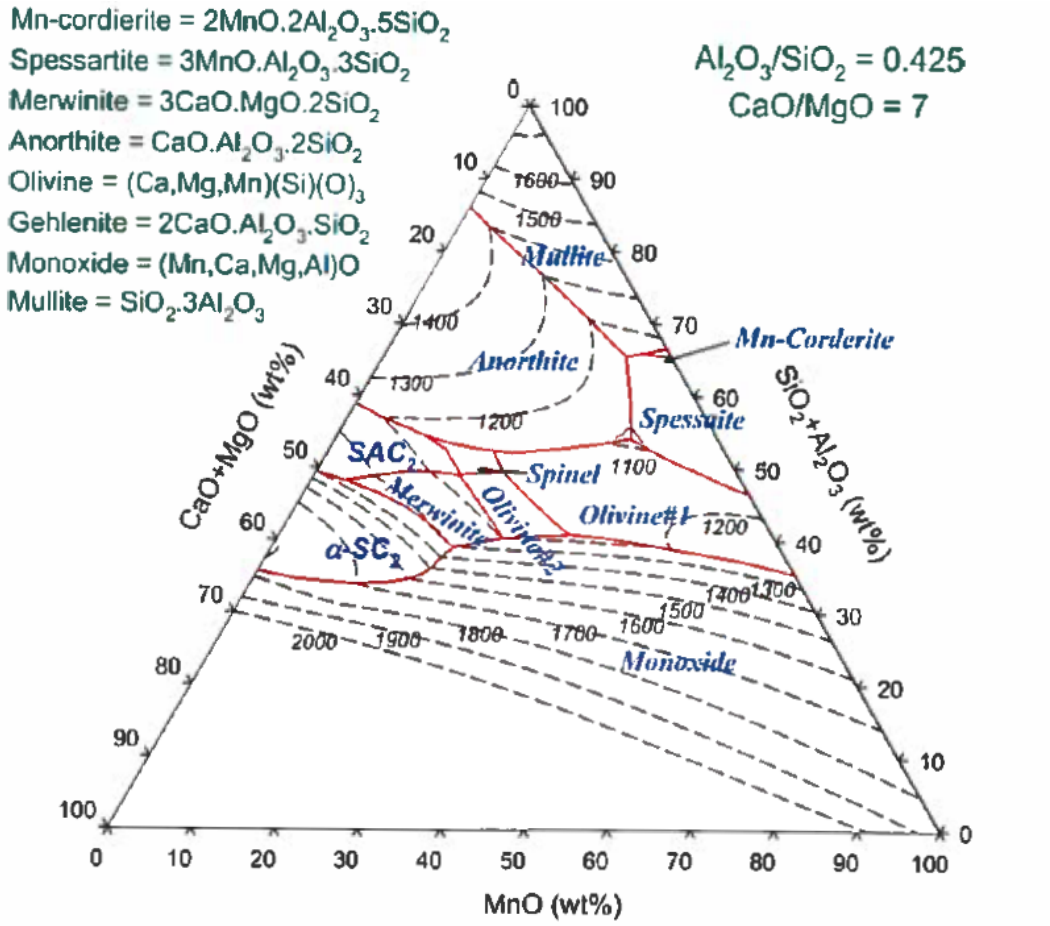

Figure 4: Calculated phase and liquidus relations for the MnO-SiO_2-CaO-Al_2O_3-MgO-system. (Al_2O_3/SiO_2 = 0.425)(CaO/MgO = 7) [2].

2.1.2. Reactions

The degree of reduction for both MnO and SiO_2 depends heavily on temperature, which can be derived from the ΔG° of reaction 12 and 13 [13]. A negative second term of ΔG^0, the change of entropy in the reaction, means the reaction is more likely to happen at higher temperatures. As the entropy change is stronger in reaction 13, it can be derived that the reduction of SiO_2 is more dependant on temperature than the reduction of MnO. As the first term, the enthalpy change of the reaction, is positive, one can also derive that both reactions consume heat from the furnace.

$$MnO(l) + C(s) = Mn(l) + CO(g) \qquad (\Delta G^0_{MnOred.} = 248,764 - 153.47T(J)) \tag{12}$$

$$SiO_2(l) + 2C(s) = Si(l) + 2CO(g) \qquad (\Delta G^0_{SiO_2red.} = 714,244 - 368.75T(J)) \tag{13}$$

Equation 12 and 13 can be combined to form a third reaction which specifies the slag-metal equilibrium. The reaction follows equation 14 and happens at the slag-metal interface rather than at the surface between the slag and the coke particles.

$$2MnO(l) + Si(l) = 2Mn(l) + SiO_2(l) \qquad (\Delta G^0_{SiO_2red.} = -216,716 + 61.81T(J)) \tag{14}$$

Two more reactions are considered important in the silicomanganese production process, the creation of SiO gas from liquid Si and SiO_2 as shown in equation 15 and the evaporation of liquid Mn as shown in equation 16 [14]. At temperatures below 1600 °C, these reactions can be neglected as the partial pressure of both SiO (g) and Mn (g) will be very low [15]. For simplicity, this is considered true across this work.

$$SiO_2(l) + Si(l) = 2SiO(g) \tag{15}$$

$$Mn(l) = Mn(g) \tag{16}$$

For each of reaction 12 and 13, an equilibrium constant, K, can be found through the well known correlation shown in equation 18 for a general reaction as shown in equation 17 [16].

$$\alpha A + \beta B = \theta R + \gamma S \tag{17}$$

$$K = \frac{(R)^\theta (S)^\gamma}{(A)^\alpha (B)^\beta} \tag{18}$$

This gives us the following equilibrium constants for the two reactions:

$$K_{MnO_{red}} = \frac{a_{Mn} \cdot p_{CO}}{a_{MnO} \cdot a_C} \tag{19}$$

$$K_{SiO_{2red}} = \frac{a_{Si} \cdot p_{CO}^2}{a_{SiO2} \cdot a_C^2} \tag{20}$$

Where K_i is the equilibrium constant for reaction i, a_j is the activity for species j and p_k is the partial pressure for species k.

As we have solid carbon present, we can assume that the activity of carbon is 1 and that the partial pressure of CO is about 1 atmosphere at temperatures above 1000 °C. This simplifies equation 19 and 20 to the following:

$$K_{MnO_{red}} = \frac{a_{Mn}}{a_{MnO}} \tag{21}$$

$$K_{SiO_{2red}} = \frac{a_{Si}}{a_{SiO2}} \tag{22}$$

At equilibrium, we have that ΔG^0 = -RT ln(K) where R is the universal gas constant and T is the temperature in Kelvin, which gives us:

$$\frac{a_{Mn}}{a_{MnO}} = exp(\frac{-248,764 + 153.47T}{RT}) \tag{23}$$

$$\frac{a_{Si}}{a_{SiO2}} = exp(\frac{-714,244 + 368.75T}{RT}) \tag{24}$$

With equation 23 and 24 we can find the equilibrium activity for MnO and SiO_2 given the temperature and the activity of Mn and Si respectively.

2.1.3. Activities and gas pressure

When calculating equilibrium values, the activity is preferred compared to using concentrations. This is due to the species interacting with each other in different ways causing the effective concentration i.e. the activity, to differ from the concentration. Activities equal to the respective concentrations follows Raoult's law, while an activity above or below the concentration is called a positive or negative deviation respectively[17]. Deviation from Raoult's law is sometimes also called deviation from ideality and defined with an activity coefficient through equation 26.

$$\gamma_i = \frac{a_i}{c_i} \tag{25}$$

Here, γ_i denotes the activity coefficient, a_i denotes the activity, and c_i denotes the concentration of species i. All values are either by weight or by molar fraction, not mixed.

Such deviation is strongly present in both the MnO-SiO_2 and Mn-Si systems, which can be seen from several works done on the topic. Tanaka [18] investigated the Mn-Si system, while Katnelson et al. [19] investigated the Mn-C system. In both studies, the activity for both elements was calculated and the results are shown in Figure 5 and 6 which shows the activity curve for Mn and C, and Mn and Si respectively.

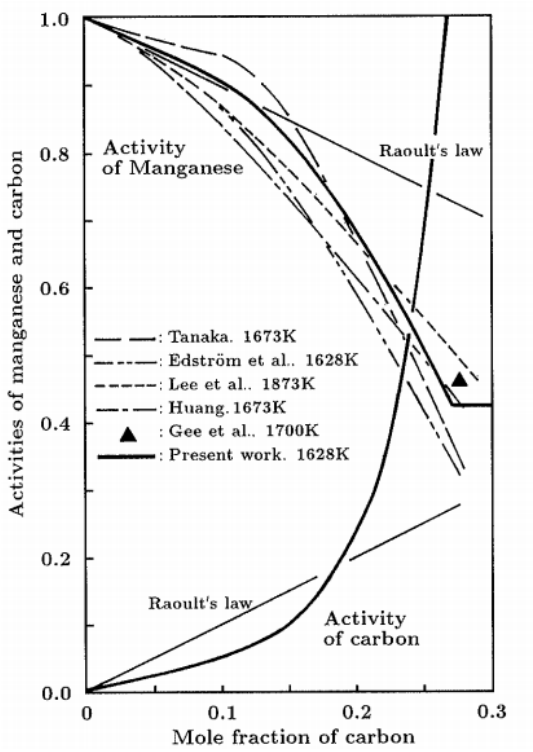

Figure 5: Activities of Mn and Si in Mn-Si melt at 1673 K[18].

The figures show that both the activities in the Mn-C system and the Mn-Si system show negative deviation from ideality. When the carbon fraction goes above 0.18 mol%, it starts showing positive deviation instead, and the activity reaches 1 at around 0.25 mol%. At this point the manganese is fully saturated with C, leading to solid particles being found in the melt. In this reference frame C is now considered to have an activity of 1.

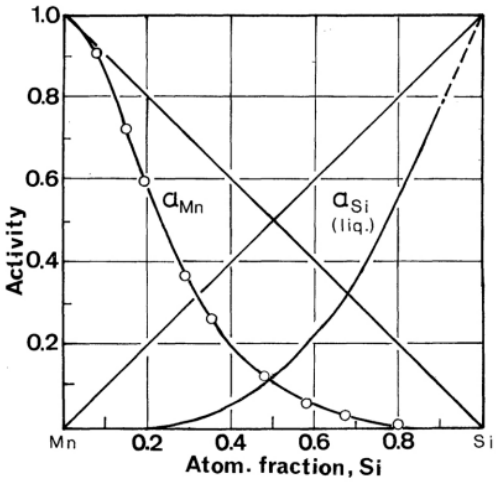

Figure 6: Activities of Mn and C in Mn-C melt at various temperatures.[19].

Kang et al. [20] did similar work on the CaO-MnO-SiO_2 and CaO-MnO-Al_2O_3 systems. The calculated iso-activity lines for MnO (with respect to the pure solid standard state) are shown in figure 7 and 8.

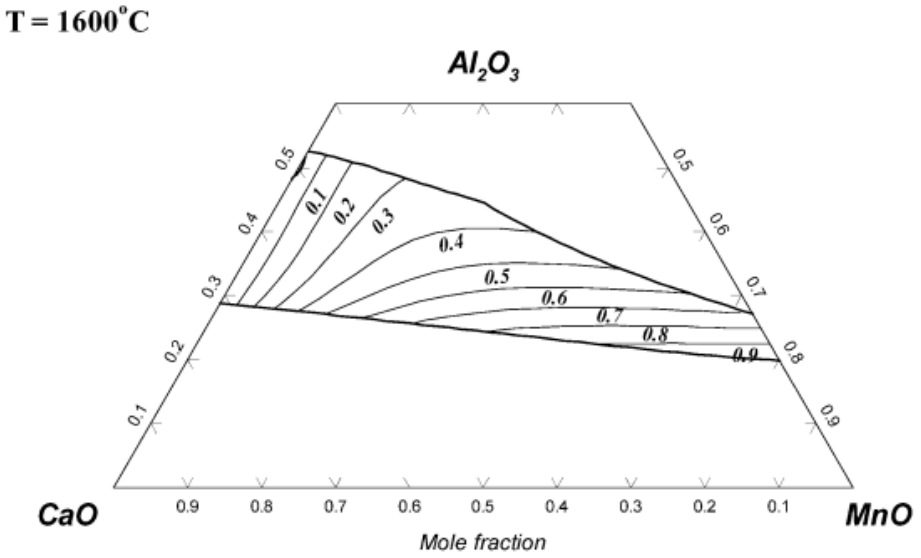

Figure 7: Calculated iso-activity lines of MnO in CaO/MnO/SiO_2 liquid solutions at 1500°C[20].

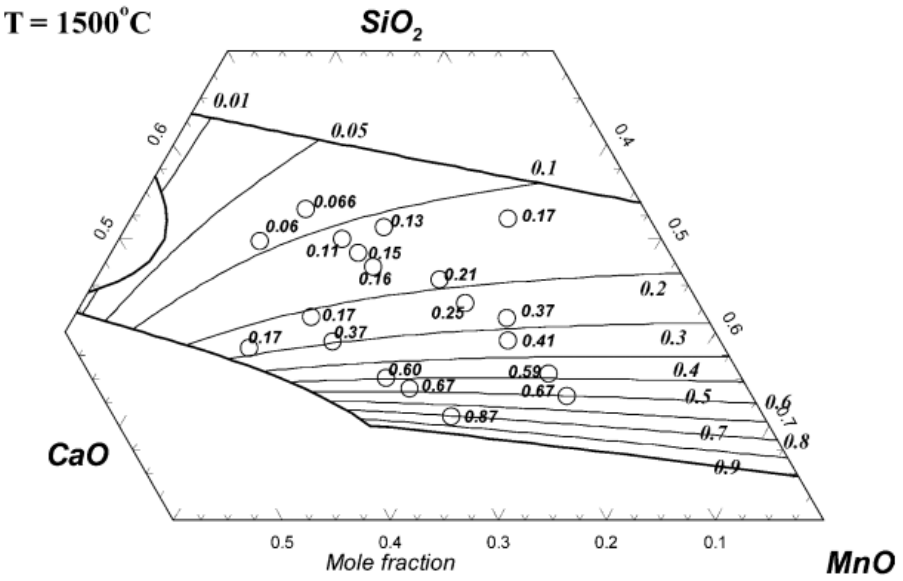

Figure 8: Calculated iso-activity lines of MnO in CaO/MnO/Al_2O_3 liquid solutions at 1600°C[20].

These figures show how CaO contributes to a positive deviation as increasing the CaO content while reducing MnO does not reduce the activity of MnO to the same degree as the lines tilt to the right or are outright flat. In contrast, Al_2O_3 and SiO_2 contribute with a negative deviation as the activity og MnO quickly decreases when the concentration of these elements are increased.

A range of such figures can be found for varying complexities of the slag and metal systems, together with formulas for the activity coefficient of various elements given the concentration of each species. Ohta and Suito [21] designed an equation for the activity coefficient of MnO using a multiple regression

analysis. Equation 26 shows the correlation between the activity of MnO and the concentration of each species as calculated by Ohta and Suito.

$$log\gamma_{MnO} = 0.019(pctCaO) + 0.023(pctMgO) - 0.023(pctSiO_2) + 0.129 \tag{26}$$

Here, pct x is the weight percent of species x and γ_i is the activity coefficient of species i.

2.2. Kinetics

It has been concluded by Brynjulfsen [3] that the chemical reaction is the rate-limiting step in the MnO-reduction process. Additionally, it has been shown that the slag and the alloy are at, or at least close to, partial equilibrium [13]. The driving force of each reaction can be described by its distance from equilibrium. For the carbothermic reactions shown in equation 12 and 13, the oxide activity is used to describe this. The driving force of a reaction i, F_i, can be written as shown in equation 27 and 28.

$$F_{MnO_{red}} = a_{MnO} - a_{MnO_{eq}} \tag{27}$$

$$F_{SiO_{2red}} = a_{SiO_2} - a_{SiO_{2eq}} \tag{28}$$

The equilibrium activity of the oxides can be found from equation 21 and 22. Combining equation 27 and 28 with equation 21 and 22 gives the formula shown in equation 29 and 30. It describes the driving force as a function of the oxide activity in the slag, as well as the activities of the corresponding metal, assuming a carbon activity and partial pressure of carbon monoxide of 1. With equation 21 and 22, this can be transcribed further, but for the ease of reading, the equilibrium constant will be used for now.

$$F_{MnO_{red}} = a_{MnO} - \frac{a_{Mn}}{K_{MnO_{red}}} \tag{29}$$

$$F_{SiO_{2red}} = a_{SiO_2} - \frac{a_{Si}}{K_{SiO_{2red}}} \tag{30}$$

Here, F_i is the driving force of reaction i, a_j is the activity of species j, $a_{j,eq}$ is the equilibrium activity of species j, and K_i is the equilibrium constant for reaction i.

2.2.1. Rate formula

The reaction rate for the carbothermic reduction reactions can be described as a function of temperature and surface area, as well as the activities of the different elements. Equation 31 shows this for the MnO-reduction.

$$r_{MnO_{red}} = f(T, A, a_{MnO}, a_C, a_{Mn}, p_{CO}) \tag{31}$$

Here, r_i is the reaction rate for reaction i in $\left[\frac{mol}{min}\right]$. This equation can similarly be made for the silicon-reducing reaction.

The reaction rate formula can be written as the temperature-dependent rate constant multiplied by the area of reaction and the driving force, as done by both Safarian [14] and Brynjulfsen [3]. With the assumption that the partial pressure of CO is 1 atm and the activity of carbon is 1, the following formula for the reaction rate of the MnO-reduction is procured, shown in equation 32. This approximation is expected to be very close to reality in most cases [5].

$$r_{MnO_{red}} = k_{0,MnO_{red}} A \cdot exp\left(-\frac{E_{A,MnO_{red}}}{RT}\right)(a_{MnO} - \frac{a_{Mn}}{K_{MnO_{red}}}) \tag{32}$$

Where A is the reaction area, $E_{A,i}$ is the activation energy, $k_{0,i}$ is the pre-exponatial rate-constant, K_i is the equilibrium constant, and r_i is the reaction rate for reaction i. Similarly, for the silica reduction we get the formula shown in equation 33.

$$r_{SiO_{2red}} = k_{0,SiO_{2red}} A \cdot exp\left(-\frac{E_{A,SiO_{2red}}}{RT}\right)(a_{SiO_2} - \frac{a_{Si}}{K_{SiO_{2red}}}) \tag{33}$$

Since the activity of a species can be described as a function of the different elements in the melt, both for the metal and for the slag, equation 32 and 33 both have only three unknown parameters. Assuming that the reaction area is known, along with the composition of the slag and metal as well as the temperature, only the pre-exponential rate constant and the activation energy are left, which together make up the rate constant k as shown in equation 34. They are used as the fitting parameters for the modelling in this project.

$$k = k_0 exp\left(-\frac{E_A}{RT}\right) \tag{34}$$

While the activation energy E_a has the units $\frac{J}{mol \cdot K}$, k_0's units depend on the wanted units for the reaction rate. In this project, mol/min was used for the reaction rate, and as such the rate constant have the same units. The activation energy for the MnO-reduction has been reported to lie around 350,000-370,000 J/mol based on experiments with synthetic MnO/SiO_2/CaO/Al_2O_3 slags around 1450-1550°C [1][22][23]. This value is closely tied to the standard Gibbs free energy of formation, which for MnO is -363,000 J/mol, and -856,000 for SiO_2 [24]. Based on this, it can be assumed that the activation energy for SiO_2 is around 850,000 J/mol, which is supported by the findings of Kim (2016) [6]. Olsø et al. (1998) [22] found that values for the reaction rate constant vary in the area of 1-16 mg/min· cm^2), with increasing k following an increase in temperature or decrease in basicity. The calculated values from Olsø's experiments can be seen in figure 4.

Table 4: Average k-values (mg/min· cm^2) from Olsø et al. [22]. Basicity and A/S are defined by the weight rations Basicity = $CaO/(SiO_2+Al_2O_3)$ and A/S = Al_2O_3/SiO_2 respectively.

		A/S=0.25	A/S=0.5
T (°C)	Basicity	k	k
1450	0.33	1.6	1.9
1450	0.67	1.4	1.2
1450	1	1.1	1
1500	0.33	4	3.8
1500	0.67	2.8	2.5
1500	1	2.3	2.1
1550	0.33	15.5	-
1550	0.67	9.5	-
1550	1	4.8	5

3. Method

Computational modelling can be defined as the use of mathematics, physics and computer science to study the behavior of complex systems by computer simulation. A studied system is characterized by a set of parameters which is simulated by adjusting these parameters and observing the outcome predicted by the model [25]. Creating a computational model of a given system is not necessarily very cheap and fast compared to performing a similar physical experiment, but once a model has been made, duplicating large quantities of experiments can easily be done. As a good model needs data to form a foundation, it is considered as a tool best used in unison with experimental work.

This work focuses on the use of computational modelling to find rate constants for MnO and SiO_2 reduction from a series of experiments. A single model was created in MATLAB R2016a to simulate the experiments, the method of which this model was implemented is explained in this chapter.

3.1. Filling in the blanks

Before modelling could begin, six relations had to be generated. These were: The activity of MnO, SiO_2, Mn and Si in their respective melts, the saturation level of carbon in the metal, and the rate formula for the balance reaction. To be able to model the activities accurately with realtively simple equations, it was decided to use activities only within the typical composition area used in the SiMn process.

3.1.1. Activities

To find formulas for the activities, thermodynamical data was acquired from the software FactSage 6.4. A pure liquid state was assumed in both the slag and the metal, and the metal was considered to be saturated with carbon. Over a hundred data points with different temperatures and compositions were generated, where the activity of the different elements where calculated with FactSage. Using Excel 2010, values using a generalized formula for the activity were compared to these values, and Excel's solver function was used to derive the parameters of the formulas which gave the least deviation.

The formulas for the activities are shown in equation 35 to 38, and the corresponding plots in figure 9 through 12 shows the values from FactSage compared to the ones calculated by the formula. In the formulas, T is the temperature deviation from 1500°C, and C_i is the weight fraction of species i.

$$\begin{aligned} a_{MnO} = C_{MnO} \cdot ln(&0.0007576T - 123.7C_{MnO} + 30.14C_{SiO_2} + 47.84C_{MgO} - 49.54C_{CaO} - 47.96C_{Al_2O_3} \\ &+ 122.8C_{MnO}^2 - 67.78C_{SiO_2}^2 - 46.32C_{MgO}^2 - 47.68C_{CaO}^2 + 22.51C_{Al_2O_3}^2 + 78.35C_{MnO}C_{CaO} \\ &+ 77.56C_{MnO}C_{MgO} + 176.6C_{MnO}C_{Al_2O_3} + 101.2C_{MnO}C_{SiO_2} - 71.52C_{SiO_2}C_{CaO} \\ &- 70.58C_{SiO_2}C_{MgO} + 27.35C_{SiO_2}C_{Al_2O_3} + 46.00C_{SiO_2}^3 - 92.97C_{CaO}C_{MgO} + 2.440C_{CaO}^3) \end{aligned} \tag{35}$$

$$a_{SiO_2} = C_{SiO_2} \cdot ln(-0.0003408T + 113.8C_{MnO} - 22.79C_{SiO_2} - 51.63C_{MgO}52.44C_{CaO} + 36.30C_{Al_2O_3} - 119.3C^2_{MnO} + 42.56C^2_{SiO_2} + 32.25C^2_{MgO} + 30.12C^2_{CaO} - 26.26C^2_{Al_2O_3} - 82.725C_{MnO}C_{CaO} - 82.90C_{MnO}C_{MgO} - 155.2C_{MnO}C_{Al_2O_3} - 86.98C_{MnO}C_{SiO_2} + 86.21C_{SiO_2}C_{CaO} + 86.19C_{SiO_2}C_{MgO} - 23.06C_{SiO_2}C_{Al_2O_3} - 31.26C^3_{SiO_2} + 69.45C_{CaO}C_{MgO} + 11.29C^3_{CaO}) \quad (36)$$

$$a_{Mn} = C_{Mn} \cdot ln(0.0005382T - 37.41C_{Mn} - 2.966C_{Si} - 0.6835C_{Fe} + 39.52C^2_{Mn} - 1.453C^2_{Si} - 0.5561C^2_{Fe} + 27.48C_{Mn}C_{Si} + 38.69C_{Mn}C_{Fe} + 0.2140C_{Si}C_{Fe}) \quad (37)$$

$$a_{Si} = C_{Si} \cdot ln(0.002464T + 10.30C_{Mn} - 1.081C_{Si} + 27.52C_{Fe} - 15.49C^2_{Mn} - 3.713C^2_{Si} - 34.66C^2_{Fe} + 1.324C_{Mn}C_{Si} - 47.01C_{Mn}C_{Fe} - 9.127C_{Si}C_{Fe}) \quad (38)$$

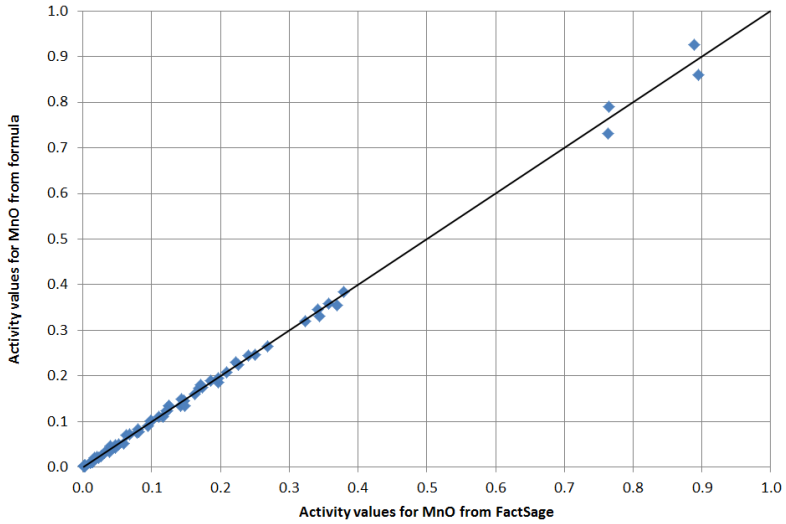

Figure 9: Comparison between the MnO activity values calculated with the formula in equation 35 and the ones calculated by FactSage

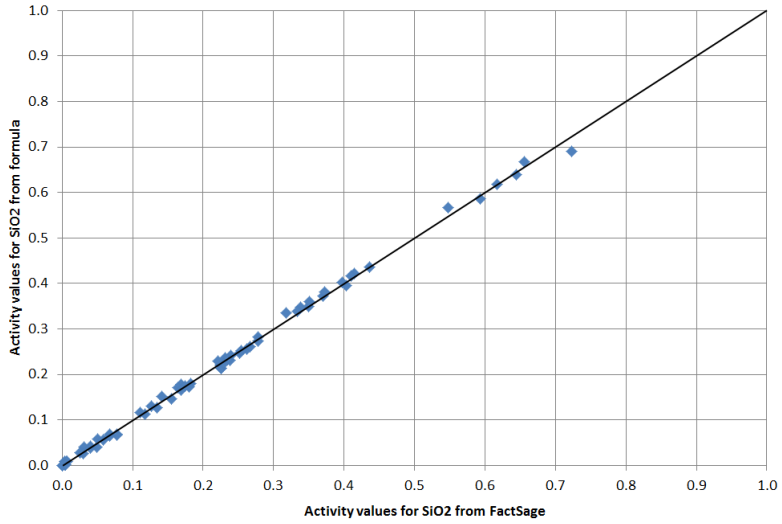

Figure 10: Comparison between the SiO_2 activity values calculated with the formula in equation 36 and the ones calculated by FactSage

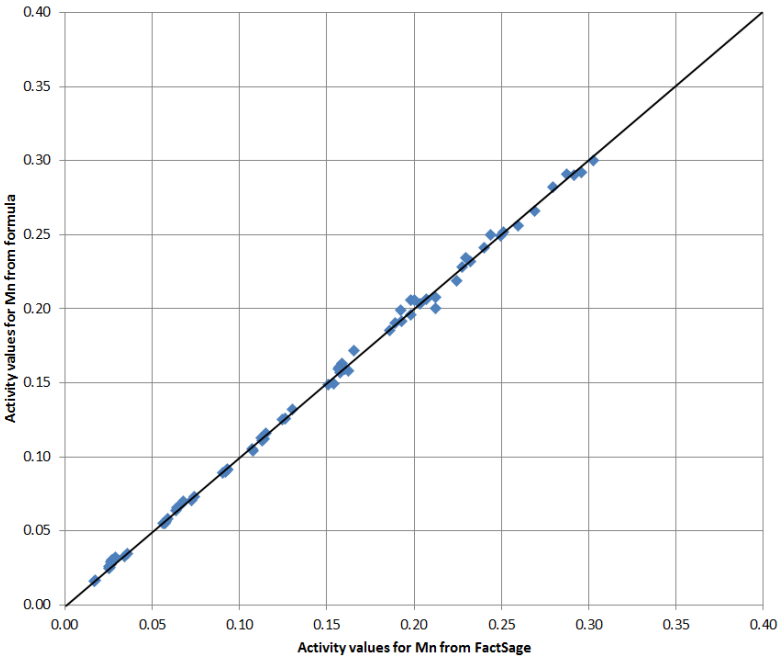

Figure 11: Comparison between the Mn activity values calculated with the formula in equation 37 and the ones calculated by FactSage

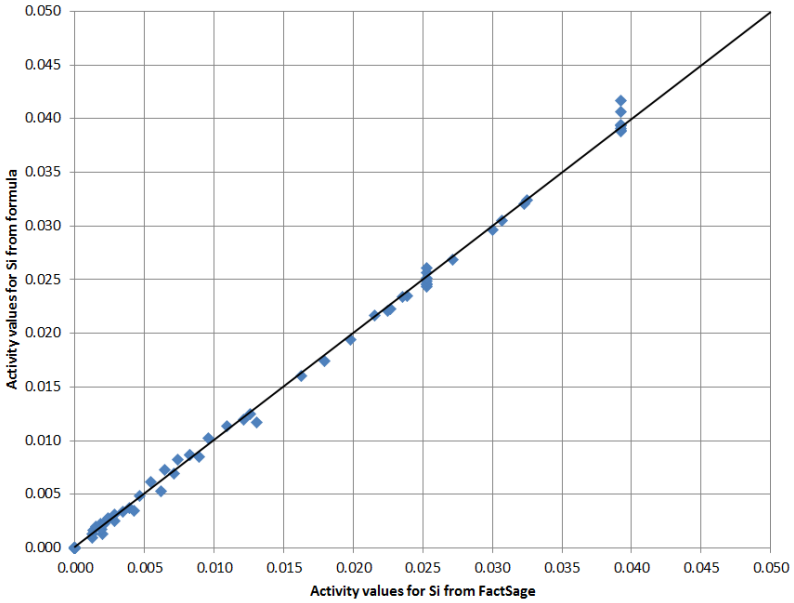

Figure 12: Comparison between the Si activity values calculated with the formula in equation 38 and the ones calculated by FactSage

The ranges of the different variables that were used to generate the formulas are shown in table 5 and 6. The formula shows a high accuracy of calculating the activity within these ranges, only showing a slightly larger deviation for the four data points seen to the top right in figure 9 where the concentration of MnO was above 80wt%. During the part of the SiMn production process that this work is modelling, the composition of the slag and metal stays well within this range. For reference, figure 13 shows the varying composition of the slag and metal during the simulation of a typical experiment. The figure shows how the concentrations of the different elements changes during a simulations in the slag and metal phases.

Table 5: Ranges of concentration for the different slag compositions which were used for generating the activity formulas shown in equation 35 and 36

Variable	T (°C)	C_{MnO}	C_{SiO_2}	C_{MgO}	C_{CaO}	$C_{Al_2O_3}$
Min	1500	0	0.2	0	0	0
Max	1600	0.6	0.55	0.2	0.4	0.2

Table 6: Ranges of concentration for the different metal compositions which were used for generating the activity formulas shown in equation 37 and 38

Variable	T (°C)	C_{Mn}	C_{Si}	C_{Fe}	C_C
Min	1500	0	0	0.1	saturated
Max	1600	0.65	0.2	0.9	saturated

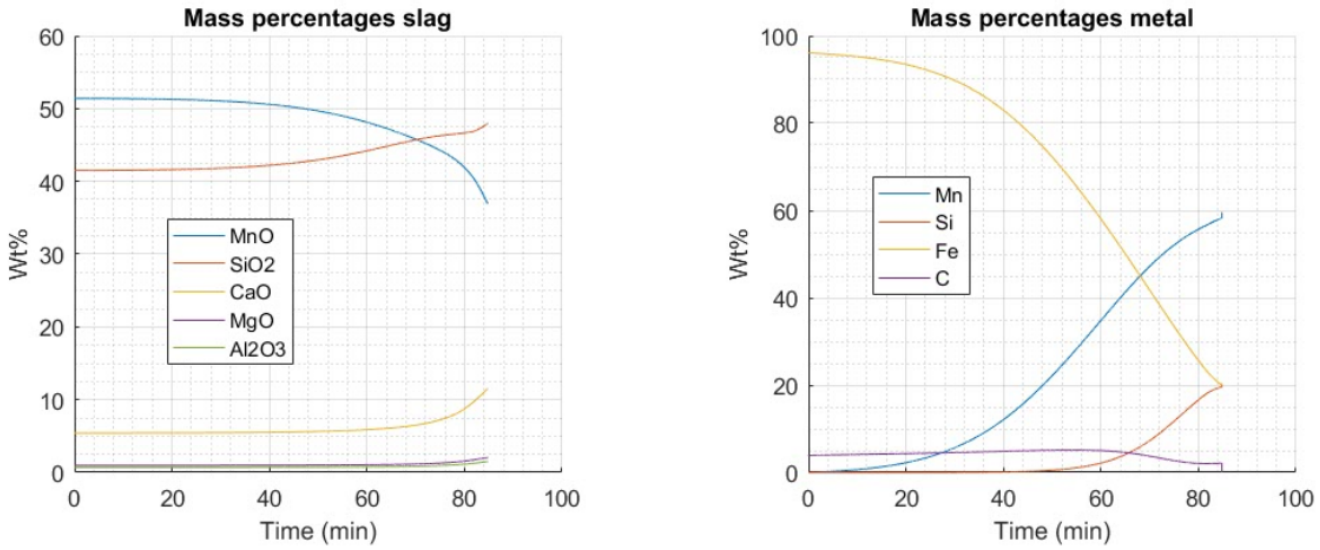

Figure 13: Composition of the slag and metal during the simulation of a typical experiment. The values are from the modelling of experiment Peace 2 curve fit.

3.1.2. Carbon saturation

In all the experiments that were evalueted, the metal was considered saturated with carbon. By using values for carbon saturation levels from FactSage, a formula for the carbon saturation was procured in similar fashion as for the activity formulas. The formula is shown in equation 39 and is considered valid for Si concentrations up to 20 wt%, Mn concentrations up to 70 wt% and temperatures between 1500°C and 1600°C. Here, C_{Si}, C_{Fe} and C_{Mn} are the weight fractions of Si, Fe and Mn in the metal respectively, and T is the temperature deviation from 1500°C. Figure 14 shows a comparison between the values from FactSage and the values calculated with the formula shown in equation 39.

$$C_{sat} = (1 + 0.00071505 \cdot T) \cdot (C_{Mn} \cdot 0.075287 - C_{Si} \cdot 0.30008 + C_{Fe} \cdot 0.051810 - C_{Si}^2 \cdot 0.17998 C_{Si}^3 \cdot 4.1373);\ [wt\%] \tag{39}$$

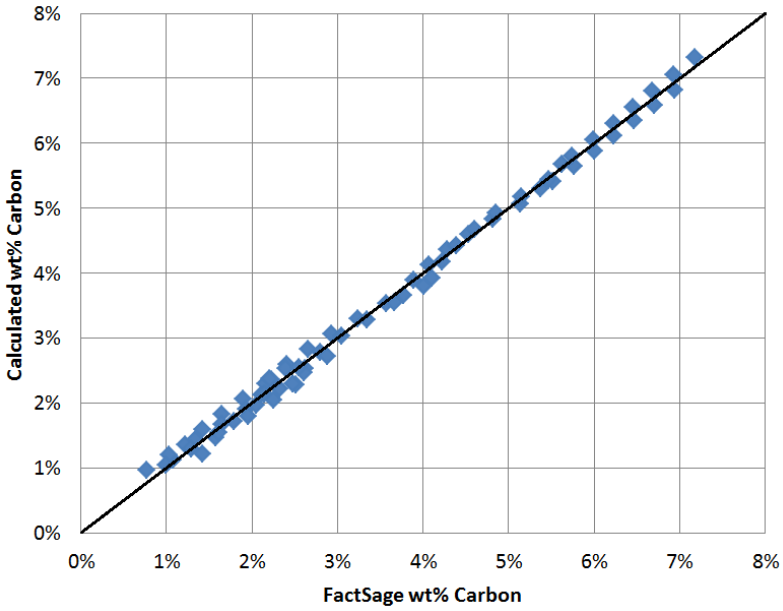

Figure 14: Comparison between carbon saturation values from FactSage and those calculated by the formula shown in equation 39.

3.2. Modelling

Using the rate formula for each of the two carbothermic reduction reactions, the SiMn-production system was modelled mathematically. This was done in MATLAB R2016b, where the reduction period was divided into discrete time-steps. As the model was matched up against experimental data, temperatures and reaction areas was taken from the experimental parameters, as was the initial composition and mass of the slag and metal used. The initial values used were taken from after pre-reduction, but before any further reaction had happened.

3.2.1. Assumptions

For this model, the partial pressure of CO, as well as the activity of carbon, is considered to be 1. The slag is assumed to be free of impurities, consisting of only MnO, SiO_2, CaO, MgO and Al_2O_3, while the metal similarly is assumed to consist of purely Mn, Si and Fe, saturated with carbon. The concentrations are assumed to lie within the limits shown in table 5 and 6, for which the activity formulas apply. It is furthermore assumed that no reduction of MnO or SiO_2 happens during pre-reduction, and that the sample is cooled fast enough after the experiment is completed, such that there is no further reactions happening after the experiment/simulation has ended. The possibility of back-reduction is discussed in section 5. Furthermore, the slag-metal equilibrium is considered balanced through equation 12 and 13 and as such, equation 14 is used.

3.2.2. The model, step by step

To generate the simulations of the experiments, the model goes through several steps:

- The experimental data is imported from an excel file. This includes the temperature, reaction area, weight loss, and time passed for each point of measurement done by the individual researcher, as well as the concentrations of the species in both slag and metal before and after reduction, but always after pre-reduction.

- Empty matrices are generated for each value that will be used throughout the model. The length of each matrix is defined by the frequency (1/second) and the length of the experiment simulated. These matrices include the temperature, area, masses, mass fractions, activities, equilibrium constants, rate of reaction, cumulative weight loss and weight loss per time.

- Initial masses are set to match the experimental data and the temperature and area curves used by the model are linearly interpolated from the experimentally provided data. This is done because the frequency of the model is higher than the experimental measurements, which is done to ensure no loss of accuracy from lack of frequency.

- Model parameters are chosen, these values are changed manually between each simulation, but the process could be made automatic after a desired error function has been implemented.

- The model goes through the matrices step-by-step, calculating the values for the next step using the known values from the current step. This is where the reaction rate formula is used to calculate the amount of slag that is reduced which decides the total masses and concentrations during the next time step. The formulas for activities and carbon concentrations are also used here, and the values seen in the graphs in chapter 4 are generates here as well.

- The generated data are plotted and the end results are printed so that the user can evaluate the results. After this step, the parameters must be changed again if results are not satisfactory, but this could be done automatically until the error reaches a certain threshold in the future.

3.2.3. Validation

The model has four parameters that was varied to make the model fit experimental data: The activation energy of the two reactions, $E_{a,1}$ and $E_{a,2}$, and the pre-exponential rate coefficients, $k_{0,1}$ and $k_{0,2}$.

The activation energy for the MnO reduction reaction, E˙a,˙Mn, is found from reversing the Arrhenius equation as done by Safarian(2007). The values vary between sets of data however, and as such a value in the middle of the most common range was chosen, 350,000 J/mol. The activation energy for the SiO_2 reduction reaction, E

Adjustments to these variables were made to allow for a best possible match when the resulting masses and mass fractions were compared to the experimental data. No automatic error calculations was performed, and the parameters were such manually adjusted. The experimental data that was used as validation is primarily the analysed end slag and metal concentrations, but also the wight loss measured during the experiments performed. A simplified error value based purely off the end concentrations generated by the model compared to the experimental data was used to assist in this. The error value for slag and metal is separately defined through equation 41 and 42 respectively, both using equation 40 as a base.

$$ErrorValue_i = (100 * C_{i,exp} - 100 * C_{i,mod})^2 \tag{40}$$

$$ErrorValueSlag = ErrorValue_{MnO} + ErrorValue_{SiO_2} \tag{41}$$

$$ErrorValueMetal = ErrorValue_{Mn} + ErrorValue_{Si} \tag{42}$$

Here, ErrorValue$_i$ is the error value for species i, $C_{i,exp}$ is the end weight fraction of species i from experimental data, and $C_{i,mod}$ is the end weight fraction of species i from the model.

4. Results

The measured starting and ending concentrations and mass for each experiment modelled can be seen in table 7 and 8 respectively. These values are from Kim(2016)[6], Holtan(2016)[7], and Skjervheim(1994)[8] and the method used to acquire the data can be studied further in their works. Only the main reduction stage was studied in this work, and as such, the starting concentration is found by assuming coplete pre-reduction of the charge. All MnO_x reduced to MnO and all FeO_x reduced to Fe. The end concentrations procured by the model are shown in table 9, while the parameter fitting used to achieve those values is discussed further in the next subsection.

Table 7: Starting concentrations (wt%) and masses for the experiments from Kim(2016), Holtan(2016) and Skjervheim(1994) after pre-reduction.

Experiment	C MnO	C SiO_2	C FeO	C CaO	C MgO	C Al_2O_3	C Mn	C Si	C Fe	C Carbon	Mass slag	Mass metal
Assmang 1	81.7%	7.9%	0.0%	8.6%	1.5%	0.4%	0.0%	0.0%	100%	saturated	16.90 g	2.43 g
Assmang 2	51.4%	41.5%	0.0%	5.4%	1.0%	0.7%	0.0%	0.0%	100%	saturated	26.94 g	2.44 g
Assmang 3	42.1%	37.3%	0.0%	10.9%	3.8%	5.8%	0.0%	0.0%	100%	saturated	29.16 g	1.37 g
Comilog 1	45.3%	36.1%	0.0%	11.8%	0.4%	6.4%	0.0%	0.0%	100%	saturated	24.35 g	0.90 g
Comilog 2	45.4%	35.7%	0.0%	12.1%	0.4%	6.4%	0.0%	0.0%	100%	saturated	8.07 g	0.30 g
Comilog 3	58.0%	33.2%	0.0%	0.7%	0.2%	7.9%	0.0%	0.0%	100%	saturated	24.48 g	1.15 g
Skjervheim 70	45.0%	27.5%	0.0%	27.5%	0.0%	0.0%	0.0%	0.0%	0.0%	saturated	100.00 g	0.00 g
Skjervheim 72	60.0%	20.0%	0.0%	12.0%	0.0%	8.0%	100%	0.0%	0.0%	saturated	20.00 g	22.00 g

Table 8: Experimental end concentrations (wt%) and masses

Experiment	C MnO	C SiO_2	C FeO	C CaO	C MgO	C Al_2O_3	C Mn	C Si	C Fe	C Carbon	Mass slag	Mass metal
Assmang 1	20.8%	40.6%	0.0%	31.8%	5.5%	1.3%	82.0%	-2.0%	20.0%	0.0	4.5 g	12.2 g
Assmang 2	3.9%	57.1%	0.0%	29.9%	5.3%	3.9%	62.4%	23.2%	14.4%	0.0	4.9 g	16.9 g
Assmang 3	6.8%	48.8%	0.0%	23.6%	8.2%	12.6%	72.3%	16.5%	11.2%	0.0	13.5 g	12.2 g
Comilog 1	30.7%	45.3%	0.1%	16.9%	0.2%	6.8%	77.2%	6.3%	16.5%	0.0	97.1 g	93.9 g
Comilog 2	1.9%	41.0%	0.0%	36.6%	1.1%	19.4%	71.2%	21.1%	7.6%	0.0	2.7 g	3.9 g
Comilog 3	32.0%	44.8%	0.0%	1.7%	0.5%	20.9%	74.4%	15.8%	9.8%	0.0	9.3 g	11.7 g
Skjervheim 70	17.6%	40.8%	0.0%	41.6%	0.0%	0.0%	99.1%	0.9%	0.0%	0.0	66.1 g	26.1 g
Skjervheim 72	27.5%	32.1%	0.0%	24.2%	0.0%	16.2%	94.9%	5.1%	0.0%	0.0	9.9 g	7.6 g

Table 9: Modelled end concentrations (wt%) and masses

Experiment	C MnO	C SiO_2	C CaO	C MgO	C Al_2O_3	C Mn	C Si	C Fe	C Carbon	Mass slag	Mass metal
Assmang 1	20.9%	34.0%	37.2%	6.4%	1.5%	80.5%	0.0%	19.4%	0.0%	3.902 g	12.496 g
Assmang 2 curve fit	37.6%	47.8%	11.2%	2.0%	1.5%	59.3%	19.8%	20.9%	0.0%	13.025 g	11.695 g
Assmang 2 value fit	3.9%	57.0%	29.9%	5.3%	3.9%	62.4%	23.2%	14.4%	0.0%	4.887 g	16.943 g
Assmang 3	9.5%	47.9%	22.7%	7.9%	12.1%	71.9%	16.5%	11.6%	0.0%	14.033 g	11.807 g
Comilog 1 slag fit	30.6%	45.3%	15.2%	0.5%	8.3%	80.0%	2.4%	17.6%	0.0%	18.822 g	5.101 g
Comilog 1 metal fit	30.8%	44.3%	15.8%	0.5%	8.6%	77.2%	6.2%	16.6%	0.0%	18.211 g	5.432 g
Comilog 2	9.3%	41.5%	31.5%	1.0%	16.7%	71.4%	20.3%	8.2%	0.0%	3.112 g	3.652 g
Comilog 3	32.0%	44.8%	1.7%	0.5%	20.9%	74.4%	15.8%	9.8%	0.0%	9.297 g	11.696 g
Skjervheim 70 metal fit	19.6%	39.8%	40.6%	0.0%	0.0%	99.1%	0.9%	0.0%	0.0%	67.771 g	24.808 g
Skjervheim 70 slag fit	17.7%	40.8%	41.5%	0.0%	0.0%	99.1%	0.9%	0.0%	0.0%	66.275 g	25.969 g
Skjervheim 72	27.7%	31.8%	24.3%	0.0%	16.2%	98.6%	1.4%	0.0%	0.0%	9.883 g	29.573 g

The experimental end concentrations seen in table 8 are taken from the experimental data provided by Skjervheim, Kim and Holtan. The modelled end concentrations are the result of the most successful simulation of each experiment. The model continuously generates masses and concentrations throughout the simulations, and the values at the end of the simulations are what is shown here.

4.1. Fitting and error

To produce the modelling results shown above, the fitting parameters were adjusted to achieve as close a representation of the original experiment as possible. Three different goals were used to judge how close the simulation came when adjusting parameters:

- The difference in end slag concentration between the experimental measurements and the model
- The difference in end metal concentration between the experimental measurements and the model
- The difference in the mass loss curve between the experimental measurements and the model

For the modelling of each experiment, reaching a low difference in all three categories was attempted. With several of the experiments however, this was not possible. In these cases, more than one set of parameters was acquired, all which can be found in table 11. Possible reasons for these discrepancies are discussed in the individual subsections for each experiment. The degree of failure in regards to the two first goals were described through the quadratic formulas described in equation 40 through 42. The resulting error values for each experiment are shown in table 10, where modelled experiments with error values below 1 can be considered to be very close to the actual experiment.

Table 10: Comparison of the experimental and modelled end concentrations, and degrees of error. Error values below 1 can be considered very good.

	C MnO		C SiO_2		C Mn		C Si		Error value	
Experiment	Exp.	Model	Exp.	Model	Exp.	Model	Exp.	Model	Slag	Metal
Assmang 1	20.8%	20.9%	40.6%	34.0%	82.0%	80.5%	-2.0%	0.0%	43.57	6.25
Assmang 2 curve fit	3.9%	37.6%	57.1%	47.8%	62.4%	59.3%	23.2%	19.8%	1222.18	21.17
Assmang 2 value fit	3.9%	3.9%	57.1%	57.0%	62.4%	62.4%	23.2%	23.2%	0.01	0.00
Assmang 3	6.8%	9.5%	48.8%	47.9%	72.3%	71.9%	16.5%	16.5%	8.10	0.16
Holtan 1 slag fit	30.7%	30.6%	45.3%	45.3%	77.2%	80.0%	6.3%	2.4%	0.01	23.05
Holtan 1 metal fit	30.7%	30.8%	45.3%	44.3%	77.2%	77.2%	6.3%	6.2%	1.01	0.01
Holtan 2	1.9%	9.3%	41.0%	41.5%	71.2%	71.4%	21.1%	20.3%	55.01	0.68
Holtan 3	32.0%	32.0%	44.8%	44.8%	74.4%	74.4%	15.8%	15.8%	0.00	0.00
Skjervheim 70 metal fit	17.6%	19.6%	40.8%	39.8%	99.1%	99.1%	0.9%	0.9%	5.00	0.00
Skjervheim 70 slag fit	17.6%	17.7%	40.8%	40.8%	99.1%	99.1%	0.9%	0.9%	0.01	0.00
Skjervheim 72	27.5%	27.7%	32.1%	31.8%	94.9%	98.6%	5.1%	1.4%	0.13	27.38

4.2. Parameters

The best attainable simulation of each experiment was performed by adjusting the parameters $k_{0,Mn}$ and $k_{0,Si}$, and a set of graphs showing the results of these simulations can be seen in figure 19 through 29. The parameters chosen for the models are shown in table 11, and the significance of these values will be further discussed in the next section. Included is the assumed area of contact between the slag and the carbon, both coke and graphite walls. This value was approximated as explained in section 3, but for experiment Skjervheim 70 and 72, it was continuously measured and as such can be varied throughout the experiment to best represent the actual experiment.

The graphs in figure 15 through 17 shows the different k_0-values in comparison to eachother for each set of experiments. It can be noticed that in the experiments where foaming was observed, the k_0 is greatly increased compared to the others, which tells us that rate of reaction is higher in these experiments. This is mostly noticeable for MnO-reduction, but a similar increase is seen for SiO_2 reduction as well. This effect is further discussed in the next subsection, as it is important when interpreting the results.

Table 11: Modelling parameters

Experiment	$k_{0,Mn}\ (mol/(s*cm^2))$	$k_{0,Si}\ (mol/(s*cm^2))$	$E_{a,Mn}\ (J/mol)$	$E_{a,Si}\ (J/mol)$	$Area(cm^2)$
Assmang 1	13,825	346	350,000	850,000	78.5
Assmang 2 curve fit	103,686	20,737	350,000	850,000	78.5
Assmang 2 value fit	282,257	56,451	350,000	850,000	78.5
Assmang 3	426,266	28,418	350,000	850,000	78.5
Comilog 1 slag fit	20,737	576	350,000	850,000	162.0
Comilog 1 metal fit	20,737	1,728	350,000	850,000	162.0
Comilog 2	28,802	96,006	350,000	850,000	54.5
Comilog 3	30,875	751	350,000	850,000	128.0
Skjervheim 70 metal fit	24,193	8,961	350,000	850,000	32.4-37.6
Skjervheim 70 slag fit	33,410	6,960	350,000	850,000	32.4-37.6
Skjervheim 72	12,673	74,546	350,000	850,000	10.5-13.2

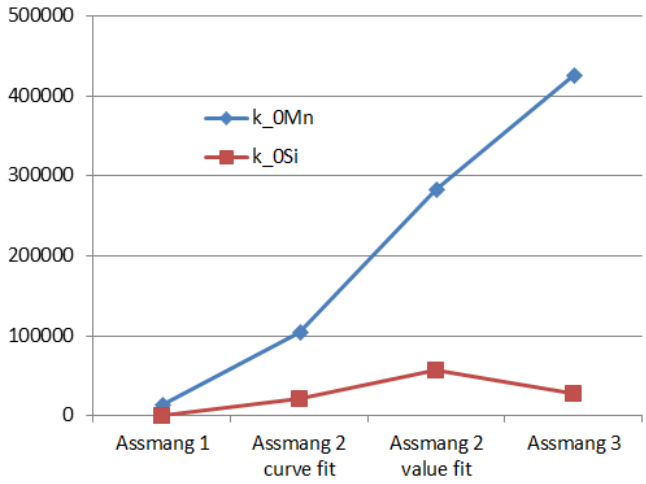

Figure 15: Values for the $k_{0,MnO}$ and k_{0,SiO_2} parameters adjusted to fit the Assmang experiments. The parameters for the second experiment were fitted once to match the mass loss curve, and once to match the end slag and metal concentrations.

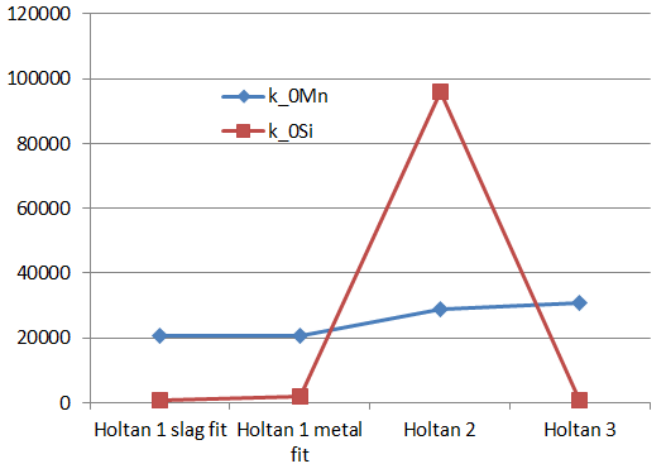

Figure 16: Values for the $k_{0,MnO}$ and k_{0,SiO_2} parameters adjusted to fit the Comilog experiments. The parameters for the first experiment were fitted once to match the end slag concentrations, and once to match the end metal concentrations.

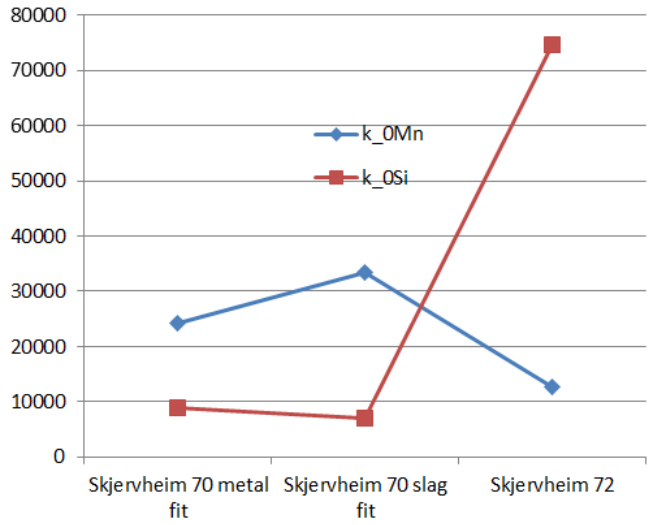

Figure 17: Values for the $k_{0,MnO}$ and k_{0,SiO_2} parameters adjusted to fit the Skjervheim experiments. The parameters for the 70-experiment were fitted once to match the end slag concentrations, and once to match the end metal concentrations.

4.3. Foaming and mass loss

In several of the experiments performed by Kim and Holtan, slag was observed outside the crucible after the completion of the experiment. It was found likely that this was due to foaming once the gas production from the reduction reactions reached a certain level [7]. This foaming caused a sudden drop in mass to be measured by the weighting equipment used in the experiments. As this mass loss is not simulated by the model however, a difference in mass loss curves are to be expected in experiments where foaming occured. The difference in the end of the mass loss curves can be used to estimate the mass lost through foaming, and these values are shown in table 12 together with the calculated percentage of mass lost. Holtan calculated the loss of mass from foaming through mass balance calculations, and found the same values as the model [7].

Table 12: Foaming

Experiment	Foaming?	Estimated mass loss	Initial weight	Mass loss percentage
Assmang 1	No		19.33 (g)	
Assmang 2 curveFit	Yes	12 (g)	29.38 (g)	41.5%
Assmang 2 valueFit	Yes	7 (g)	29.38 (g)	24.5%
Assmang 3	Yes	13 (g)	30.53 (g)	41.6%
Comilog 1 slagFit	No		25.25 (g)	
Comilog 1 metalFit	No		25.25 (g)	
Comilog 2	Other loss	1 (g)	8.37 (g)	13.1%
Comilog 3	Yes	4 (g)	25.63 (g)	15.6%
Skjervheim70 metalFit	No		100 (g)	
Skjervheim70 slagFit	No		100 (g)	
Skjervheim72	No		20 (g)	

In addition to the direct mass loss, another consequence of foaming must be considered as previously mentioned. That is the increase of reduction speed during foaming. When the gas bubbles force the slag upwards and out of the crucible, the slag will be in contact with a much larger part of the graphite walls as well as any coke that lies above the slag. This increase in contact area will increase the reaction rate according to formula 32. This effect is illustrated in figure 18.

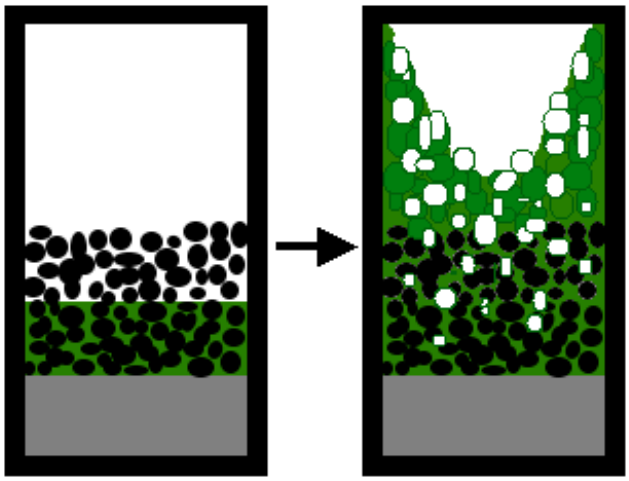

Figure 18: An illustration of the contact area increasing effect that foaming might have had on the experiments. The gray area is liquid metal, the black is the graphite walls and the coke particles, the green is slag and the white is gas. THe right picture shows the foaming.

4.4. Modelling results

Following is a series of graphs which show the progress of the reduction processes that have been modelled. The graphs show a series of values as a function of time throughout the process: the driving force of the MnO-reduction, concentrations in the slag and metal, the masses of the main elements, the mass loss in the model compared to the experimental values, the temperature, and the derivative of the weight loss. In many of the graphs, a sharp line upwards or downwards can be seen at the end of several lines, these exist because the carbon content in the metal is reduced to 0 in the final time-step. This was done so the concentrations from the model can be compared to the measurements from the experiments where the carbon also is removed as can be seen in table 8.

The speed of the weight loss is calculated by dividing the difference of each pair of mass loss values by the length of the time step between them. Because of the high degree of noise in the experimental data, the moving average is instead displayed for clarity of view. Each value shown in the graphs are the average of the value added to the fifteen preceding and following values. This was done for both modelled and experimental data, but due to the low amount of data points from Skjervheim 70 and 72, only 1 preceding and following value was used for smoothing the experimental data for these three graphs.

4.4.1. Assmang 1

Modelled values as a function of time for the experiment Assmang 1. The graphs show the driving force and its parts, the mass percentages in the slag and metal, the mass of the main species, the temperature, as well as the modelled and experimental values for mass loss and rate of mass loss. The charge in the experiment consisted of assmang ore and coke, heated to around 1605 °C. Data taken from Kim(2016) [6] and the presented model.

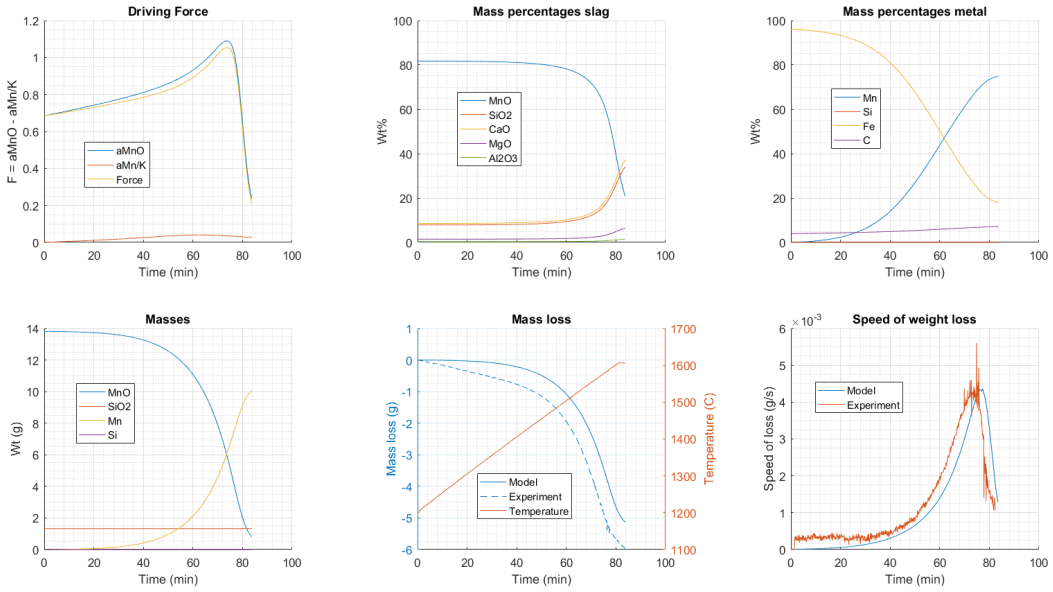

Figure 19: Graphs from the simulation of Assmang experiment 1 [6]. Graphs from top left: The different parts of the driving force of the MnO reduction reaction (aMnO - aMn/K) over time, the Mass percentages of the different slag elements over time, the mass percentages of the different elements in the metal over time, the total mass of the four main elements over time, the mass loss through CO-formation in the model compared to the measured experimental mass loss over time, the speed of weight loss over time.

It can be seen from figure 19 that the modelling of this experiment is far from perfect. The reduction starts much earlier in the experiment compared to the model, resulting in 1g more of mass loss total at the end. In this experiment it should also be noted that the concentration of SiO_2 is below the lower limit for the activity formulas introduced in section 3, which could explain the discrepancy.

4.4.2. Assmang 2 curve fit

Modelled values as a function of time for the experiment Assmang 2. The graphs show the driving force and its parts, the mass percentages in the slag and metal, the mass of the main species, the temperature, as well as the modelled and experimental values for mass loss and rate of mass loss. The charge in the experiment consisted of Assmang ore, coke, and quartz, heated to around 1605 °C. Data taken from Kim(2016) [6] and the presented model.

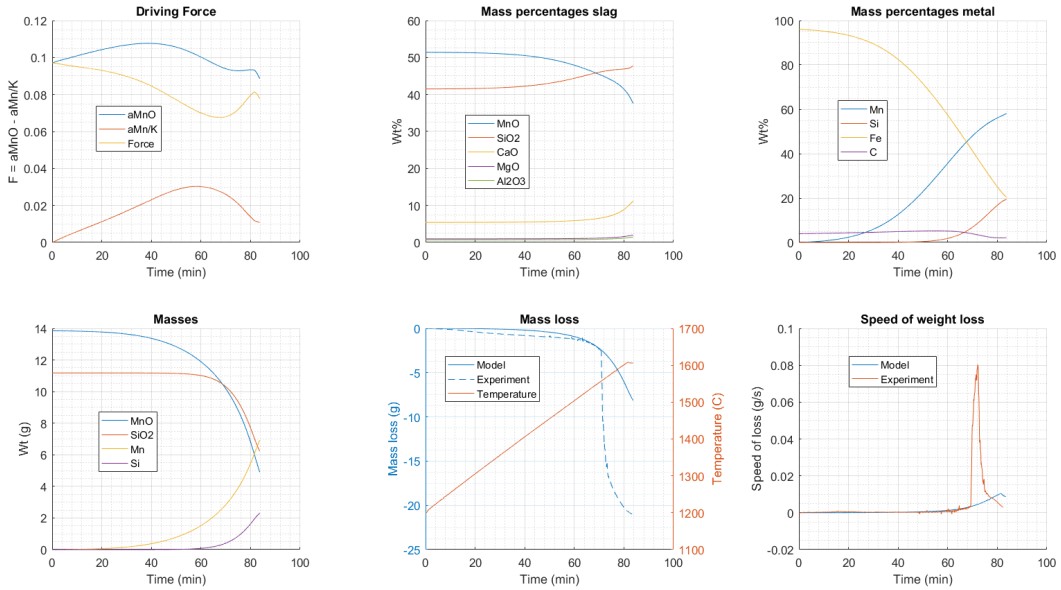

Figure 20: Graphs from the simulation of Assmang experiment 2, fitted to match the mass-loss curve [6]. Graphs from top left: The different parts of the driving force of the MnO reduction reaction (aMnO - aMn/K) over time, the Mass percentages of the different slag elements over time, the mass percentages of the different elements in the metal over time, the total mass of the four main elements over time, the mass loss through CO-formation in the model compared to the measured experimental mass loss over time, the speed of weight loss over time.

Here the parameters were adjusted to make the mass loss curve fit in the time before the foaming started. The effect of the increased reaction rate during foaming can be noticed through the last graph, as the reaction rate after the foaming is much lower for the experiment than for the model. It can be assumed that in this experiment, the actual concentration of MnO in the slag would be reduced at a quicker rate during foaming, but then flatten out in the end as the driving force is reduced.

4.4.3. Assmang 2 concentration fit

Modelled values as a function of time for the experiment Assmang 2. The graphs show the driving force and its parts, the mass percentages in the slag and metal, the mass of the main species, the temperature, as well as the modelled and experimental values for mass loss and rate of mass loss. The charge in the experiment consisted of Assmang ore, coke, and quartz heated to around 1605 °C. Data taken from Kim(2016) [6] and the presented model.

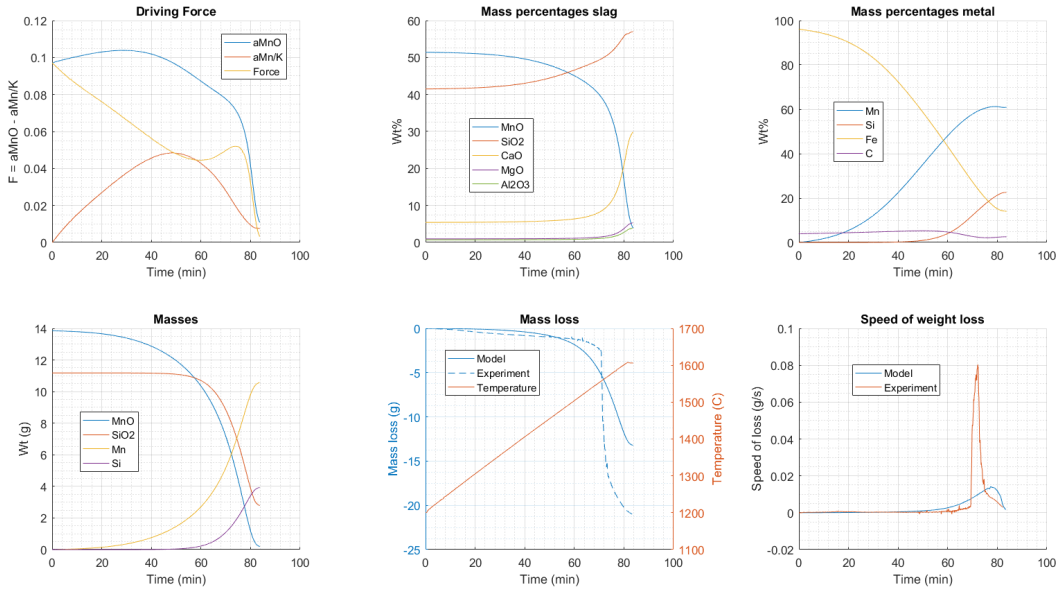

Figure 21: Graphs from the simulation of Assmang experiment 2, fitted to match the end slag concentrations [6]. Graphs from top left: The different parts of the driving force of the MnO reduction reaction (aMnO - aMn/K) over time, the Mass percentages of the different slag elements over time, the mass percentages of the different elements in the metal over time, the total mass of the four main elements over time, the mass loss through CO-formation in the model compared to the measured experimental mass loss over time, the speed of weight loss over time.

Here the parameters were adjusted to make the end concentrations match between the experiment and the model. It can be seen from the graphs that an increased base rate of reaction compared to when fitting for the curve was necessary to obtain the same products. The reaction therefore starts earlier for the model than the actual experiment, but during foaming, even higher rates are achieved, making it even out in the end.

4.4.4. Assmang 3

Modelled values as a function of time for the experiment Assmang 3. The graphs show the driving force and its parts, the mass percentages in the slag and metal, the mass of the main species, the temperature, as well as the modelled and experimental values for mass loss and rate of mass loss. The charge in the experiment consisted of Assmang ore, coke, quartz, and HCFeMn slag heated to around 1605 °C. Data taken from Kim(2016) [6] and the presented model.

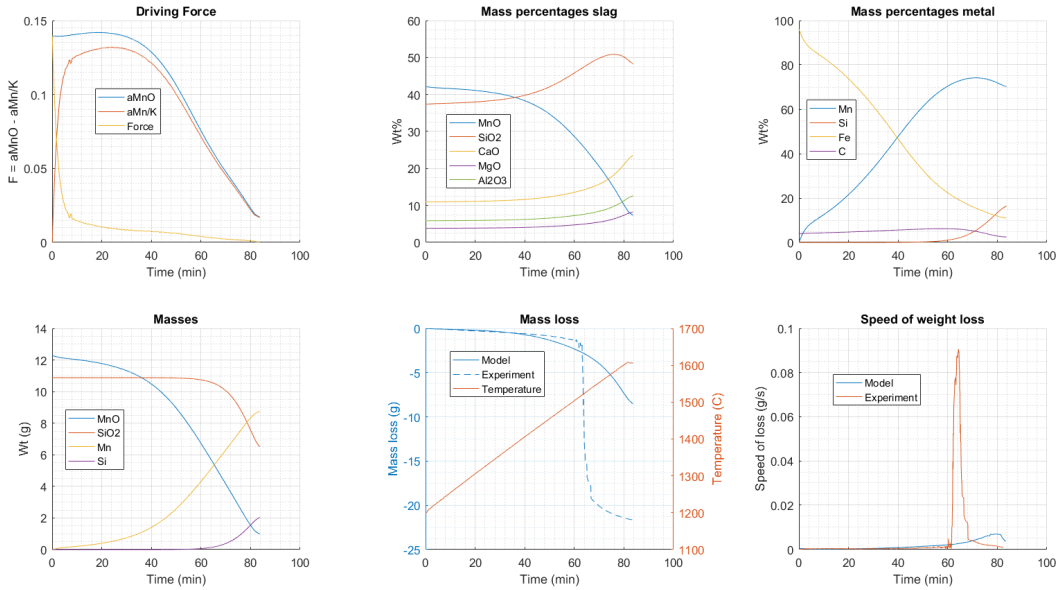

Figure 22: Graphs from the simulation of Assmang experiment 3 [6]. Graphs from top left: The different parts of the driving force of the MnO reduction reaction (aMnO - aMn/K) over time, the Mass percentages of the different slag elements over time, the mass percentages of the different elements in the metal over time, the total mass of the four main elements over time, the mass loss through CO-formation in the model compared to the measured experimental mass loss over time, the speed of weight loss over time.

Here all three criteria were fulfilled to a certain degree with one set of parameters. The curve matches well up until the foaming starts, at which point it can no longer be expected to match. After the foaming, the rate of reduction is reduced in the experimental data, but increases gradually in the model. This again points towards an increased rate of eduction during foaming, which leads to a lower MnO-content and thereby lowered driving force after the foaming.

4.4.5. Comilog 1 slag fit

Modelled values as a function of time for the experiment Comilog 1. The graphs show the driving force and its parts, the mass percentages in the slag and metal, the mass of the main species, the temperature, as well as the modelled and experimental values for mass loss and rate of mass loss. The charge in the experiment consisted of Comilog ore, coke, quartz, and limestone heated to around 1625 °C. Data taken from Holtan(2016) [7] and the presented model.

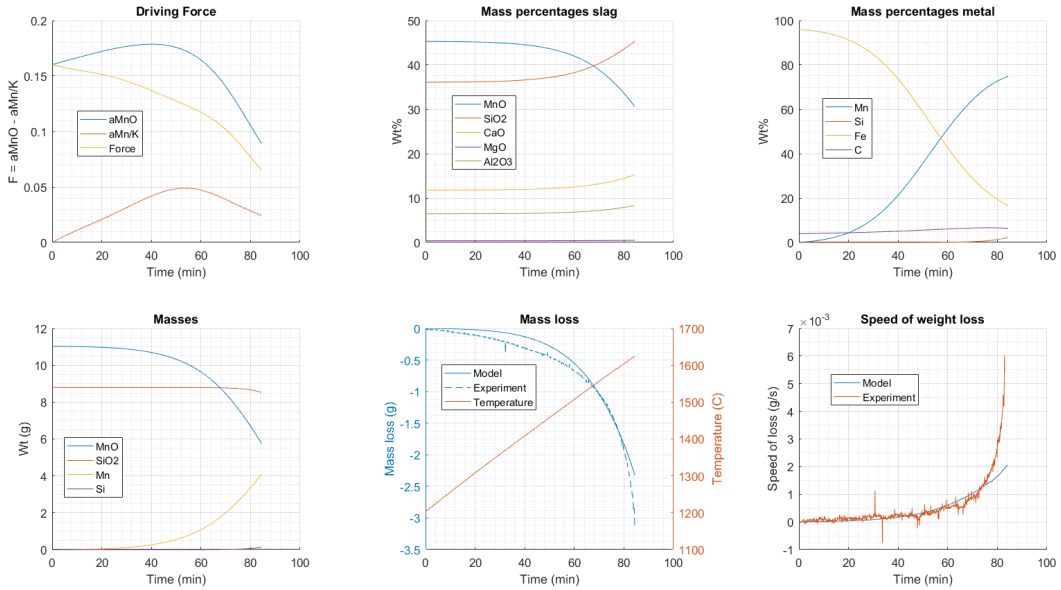

Figure 23: Graphs from the simulation of Comilog experiment 1, fitted to match the end slag concentration [7]. Graphs from top left: The different parts of the driving force of the MnO reduction reaction (aMnO - aMn/K) over time, the Mass percentages of the different slag elements over time, the mass percentages of the different elements in the metal over time, the total mass of the four main elements over time, the mass loss through CO-formation in the model compared to the measured experimental mass loss over time, the speed of weight loss over time.

Here the parameters were adjusted to make the end slag compositions match. The reduction starts much earlier in the experiment compared to the model, and it also ends with a higher mass loss rate. It can be noted that seemingly neither the model nor the experiment has reached near equilibrium here, as the rate of mass loss is increasing and the end concentration of MnO is high. In this graph, there is about a 0.5g of difference in the end mass loss.

4.4.6. Comilog 1 metal fit

Modelled values as a function of time for the experiment Comilog 1. The graphs show the driving force and its parts, the mass percentages in the slag and metal, the mass of the main species, the temperature, as well as the modelled and experimental values for mass loss and rate of mass loss. The charge in the experiment consisted of Comilog ore, coke, quartz, and limestone heated to around 1625 °C. Data taken from Holtan(2016) [7] and the presented model.

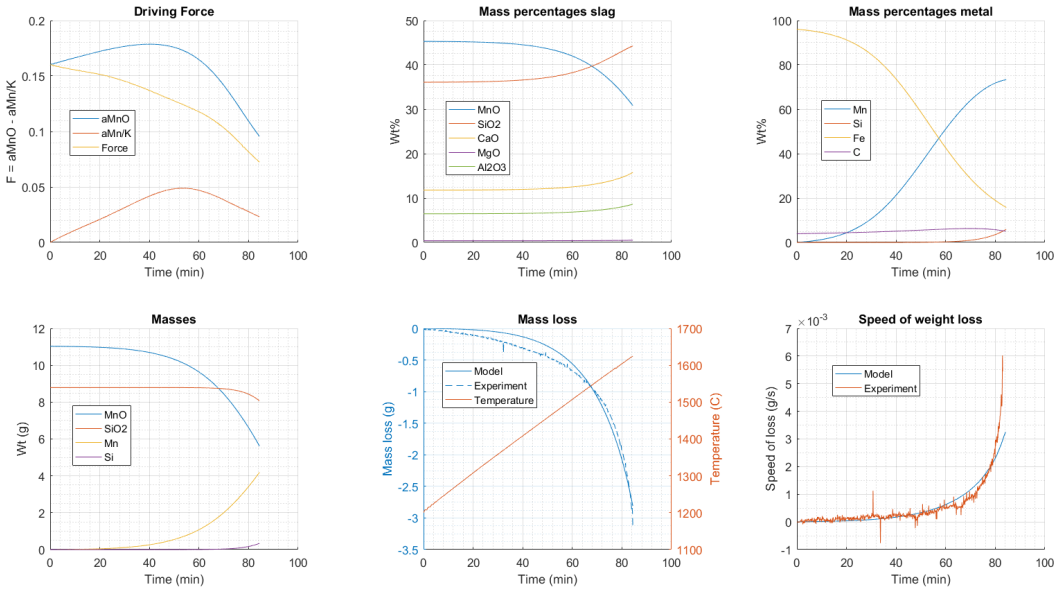

Figure 24: Graphs from the simulation of Comilog experiment 1, fitted to match the end metal concentration [7]. Graphs from top left: The different parts of the driving force of the MnO reduction reaction (aMnO - aMn/K) over time, the Mass percentages of the different slag elements over time, the mass percentages of the different elements in the metal over time, the total mass of the four main elements over time, the mass loss through CO-formation in the model compared to the measured experimental mass loss over time, the speed of weight loss over time.

Here the parameters were adjusted to make the end metal compositions match. Also here does the reaction start earlier in the experimental values, but towards the end of the experiment, the curves match very well. Neither the model nor the experiment has reached near equilibrium, as the rate of mass loss is increasing and the MnO-content in the slag is still high. In this graph there is little to no difference in the end mass loss.

4.4.7. Comilog 2

Modelled values as a function of time for the experiment Comilog 2. The graphs show the driving force and its parts, the mass percentages in the slag and metal, the mass of the main species, the temperature, as well as the modelled and experimental values for mass loss and rate of mass loss. The charge in the experiment consisted of Comilog ore, coke, quartz, and limestone heated to around 1650 °C, and with extra coke added on top of the charge to prevent foaming. Data taken from Holtan(2016) [7] and the presented model.

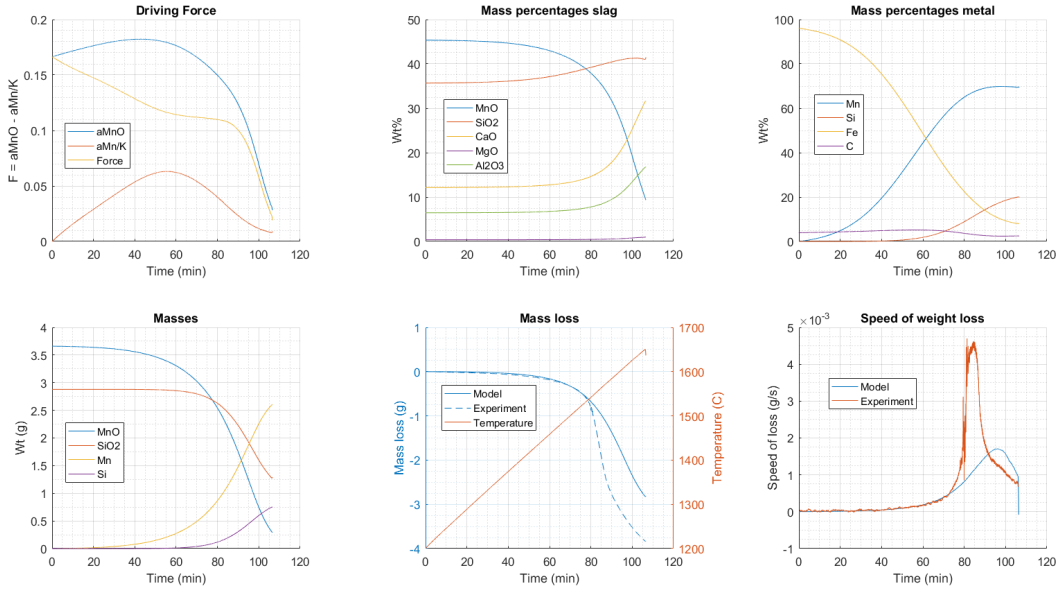

Figure 25: Graphs from the simulation of Comilog experiment 2 [7]. Graphs from top left: The different parts of the driving force of the MnO reduction reaction (aMnO - aMn/K) over time, the Mass percentages of the different slag elements over time, the mass percentages of the different elements in the metal over time, the total mass of the four main elements over time, the mass loss through CO-formation in the model compared to the measured experimental mass loss over time, the speed of weight loss over time.

Here the parameters were adjusted to fit the metal as the extremely low MnO concentration in the slag from the experiment is unreachable with the thermodynamic limitations introduced in this model. In this experiment, additional coke was added on top of the charge, which stopped any foaming from occurring. There is a difference in end mass loss of about 1g, but about half of that can be assumed to be volatiles from the added carbon that burns away [7]. The speed of mass loss is greatly increased in the period where foaming occurred in the first comilog experiment, but no foaming was observed and no similar spike of mass loss speed can be seen in the graph. Partial foaming that is suppressed below the lid could explain the increased reaction rate, which is backed by our previous observations of the reaction rate during foaming. It should also be mentioned that the increase in reaction rate during foaming and suppressed foaming not necessarily is caused by the foaming itself, but rather by some other phenomenon that is triggered by the heat and/or increased gas production.

4.4.8. Comilog 3

Modelled values as a function of time for the experiment Comilog 3. The graphs show the driving force and its parts, the mass percentages in the slag and metal, the mass of the main species, the temperature, as well as the modelled and experimental values for mass loss and rate of mass loss. The charge in the experiment consisted of Comilog ore, coke, and quartz, heated to around 1700 °C. Data taken from Holtan(2016) [7] and the presented model.

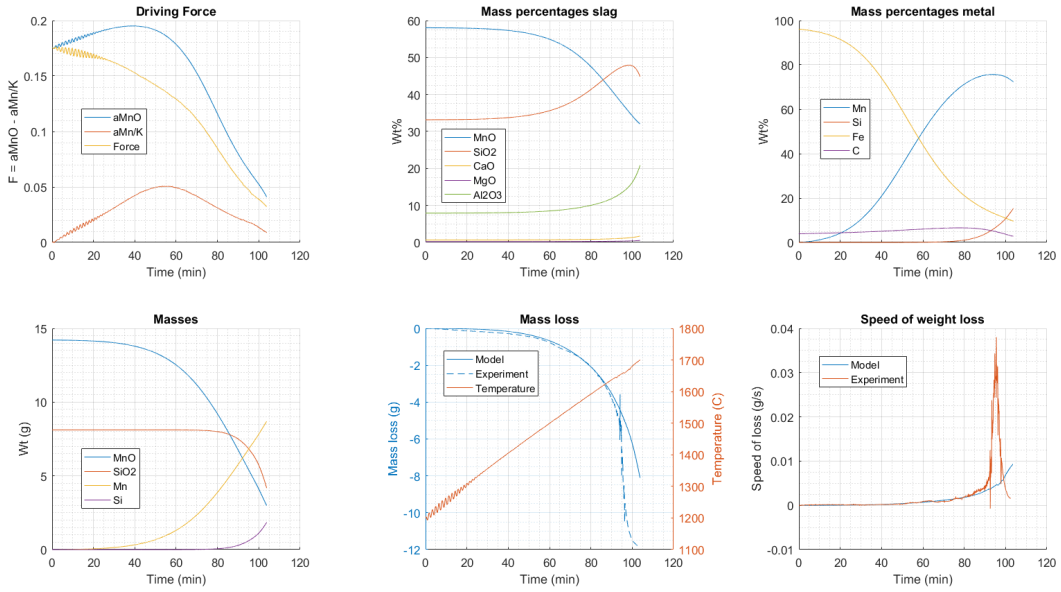

Figure 26: Graphs from the simulation of Comilog experiment 3 [7]. Graphs from top left: The different parts of the driving force of the MnO reduction reaction (aMnO - aMn/K) over time, the Mass percentages of the different slag elements over time, the mass percentages of the different elements in the metal over time, the total mass of the four main elements over time, the mass loss through CO-formation in the model compared to the measured experimental mass loss over time, the speed of weight loss over time.

Here the parameters were adjusted to fit both the metal and the slag end concentrations, as well as the curve up until foaming. In this experiment, boiling was observed and a weight loss of 4g was calculated through mass balance [7] which matches what can be seen in the mass loss graph. The spike in the weight loss speed followed by the rapid decline again follows the trend of a severely increased reacion rate during foaming with the following reduced MnO-concentration leading to a lower driving force and therefore reaction speed after the foaming.

4.4.9. Skjervheim 70 metal fit

Modelled values as a function of time for the experiment Skjervheim 70. The graphs show the driving force and its parts, the mass percentages in the slag and metal, the mass of the main species, the temperature, as well as the modelled and experimental values for mass loss and rate of mass loss. The charge in the experiment consisted of Synthetic MnO, SiO_2, and CaO, held constant at 1500 °C. Data taken from Skjervheim(1994) [8] and the presented model.

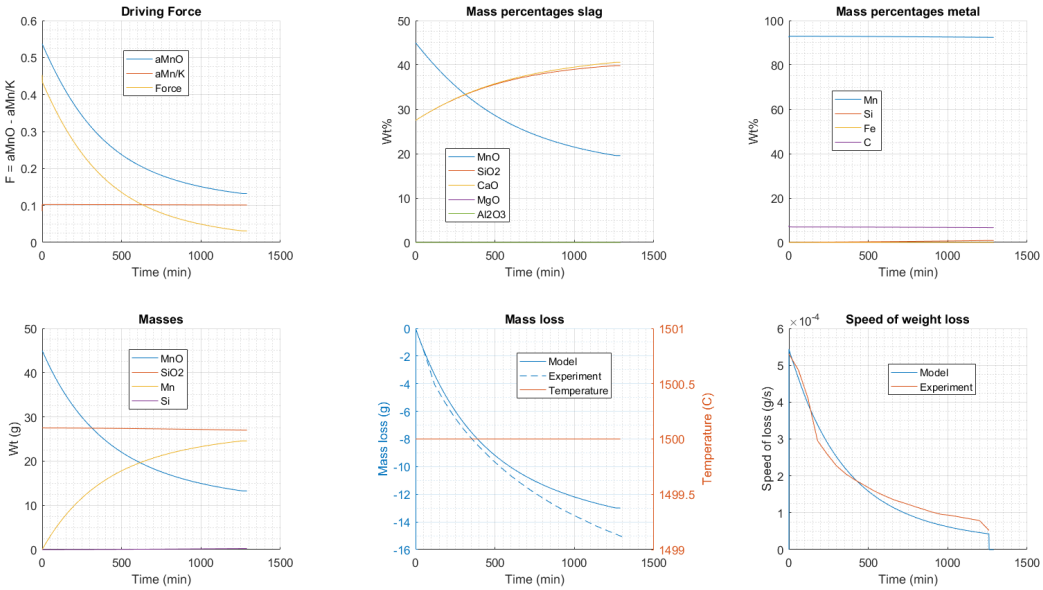

Figure 27: Graphs from the simulation of Skjervheim experiment 70, fitted to match the end metal concentration [8]. Graphs from top left: The different parts of the driving force of the MnO reduction reaction (aMnO - aMn/K) over time, the Mass percentages of the different slag elements over time, the mass percentages of the different elements in the metal over time, the total mass of the four main elements over time, the mass loss through CO-formation in the model compared to the measured experimental mass loss over time, the speed of weight loss over time.

Here the parameters were adjusted to fit the metal end concentration. This experiment is with synthetic materials and with a constant and lower temperature than the others. As there is no iron in the metal, the activity formula cannot be assumed to be accurate. The model reaches equilibrium at a higher MnO-content in the slag compared to the experiment, which might be accredited to this. The mass loss and mass loss speed curves are both quite similar between the model and the experiment apart from the earlier flattening of the model mass loss curve.

4.4.10. Skjervheim 70 slag fit

Modelled values as a function of time for the experiment Skjervheim 70. The graphs show the driving force and its parts, the mass percentages in the slag and metal, the mass of the main species, the temperature, as well as the modelled and experimental values for mass loss and rate of mass loss. The charge in the experiment consisted of Synthetic MnO, SiO_2, and CaO, held constant at 1500 °C. Data taken from Skjervheim(1994) [8] and the presented model.

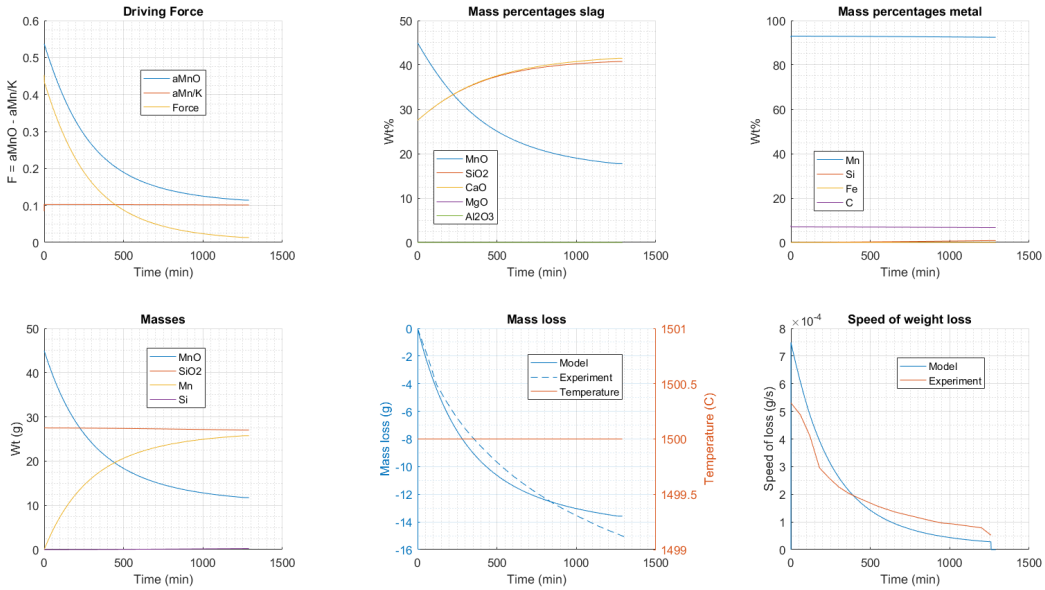

Figure 28: Graphs from the simulation of Skjervheim experiment 70, fitted to match the end slag concentration [8]. Graphs from top left: The different parts of the driving force of the MnO reduction reaction (aMnO - aMn/K) over time, the Mass percentages of the different slag elements over time, the mass percentages of the different elements in the metal over time, the total mass of the four main elements over time, the mass loss through CO-formation in the model compared to the measured experimental mass loss over time, the speed of weight loss over time.

Here the parameters were adjusted to fit the slag end concentration. This experiment is with synthetic materials and with a constant and lower temperature than the others. As there is no iron in the metal, the activity formula cannot be assumed to be accurate. The model reaches equilibrium at a higher MnO-content in the slag compared to the experiment, which might be accredited to this. The model mass loss rate starts higher here to produce a lower content of MnO in the slag, but the curve flattens out as the driving force approaches 0 when the MnO content approaches 17wt%.

4.4.11. Skjervheim 72

Modelled values as a function of time for the experiment Skjervheim 72. The graphs show the driving force and its parts, the mass percentages in the slag and metal, the mass of the main species, the temperature, as well as the modelled and experimental values for mass loss and rate of mass loss. The charge in the experiment consisted of Synthetic MnO,SiO_2, CaO, and Al_2O_3, held constant at 1500 °C. Data taken from Skjervheim(1994) [8] and the presented model.

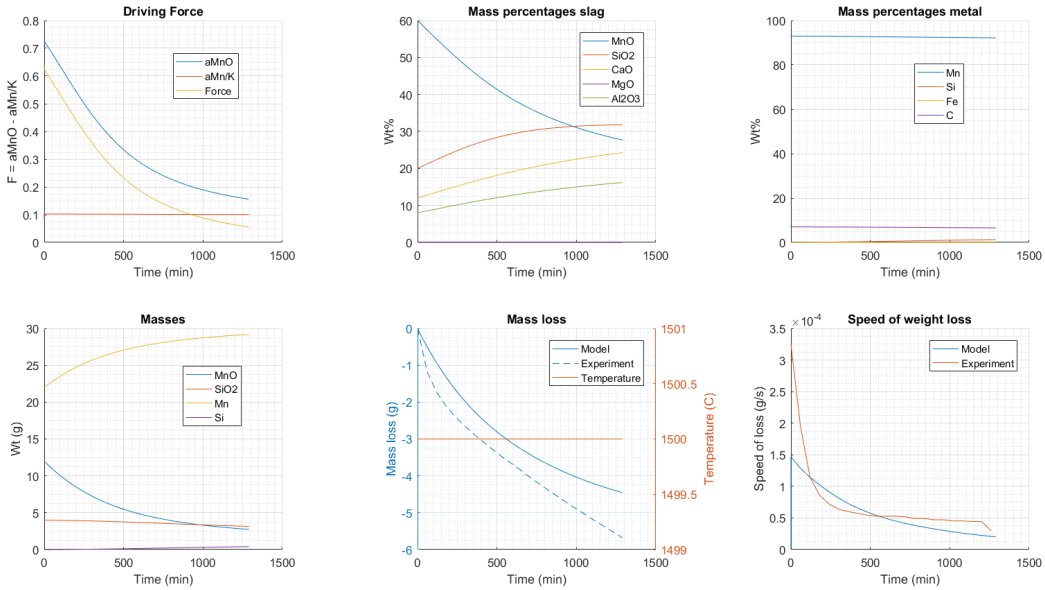

Figure 29: Graphs from the simulation of Skjervheim experiment 72[8]. Graphs from top left: The different parts of the driving force of the MnO reduction reaction (aMnO - aMn/K) over time, the Mass percentages of the different slag elements over time, the mass percentages of the different elements in the metal over time, the total mass of the four main elements over time, the mass loss through CO-formation in the model compared to the measured experimental mass loss over time, the speed of weight loss over time.

Here the parameters were adjusted to fit the slag and metal end concentration. This experiment is with synthetic materials and with a constant and lower temperature than the others. As there is no iron in the metal, the activity formula cannot be assumed to be accurate. The model reaches equilibrium at a much higher MnO-content in the slag compared to the experiment, which might be accredited to this. The experiment also produces a notable amount of Si (5wt%), which is not thermodynamically feasible with the values and assumptions used in the model. This could also be accredited to activity values that vary from the ones calculated by the formulas presented in section 3.

5. Discussions

In this section, the results will be discussed and the model data compared to the experimental data do assess its viability as well as its utility. In the subsequent three subsections, each of the three experiment sets and what might be learned from the modelling data acquired for each set will be discussed. The foaming and rapid mass loss will be discussed in it's own subsection, and lastly, possible explanations for the different errors and inaccuracies will be discussed.

5.1. Model viability and utility

Although the model doesn't manage to perfectly replicate the experimental slag, metal and mass loss curves for all the experiments, it does manage very well in many cases. Most natable is the disparity whenever foaming was observed, and since that occurred in a large number of experiments, it is something that should be considered implemented in the model. It could be possible to add a factor for the reaction rate that is dependent on the reaction rate itself.

Aside from the cases with foaming, the failed simulations were mainly from experiments that did not fit within the parameters set by the models definition. The concentrations of either the slag or the metal was outside the acceptable limits in some regard, which could lead to large errors in activity calculation. Those experiments therefore cannot be used to discredit the model, as the model by its definition should not be able to perfectly model them. These experiments are Assmang 1 and the experiments from Skjervheim, and they will not be used in the conclusions as they fall outside the boundaries of the model.

For the remaining experiments, in all but one, almost almost perfect end composition were achieved for either the slag or the metal, and for both in many cases. The experiment Holtan 2 had an extremely low MnO-content in the slag, which the model could not replicate, but the special case of

Assuming that the model is correct in the remaining cases, the information one can get from it can be very valuable. Knowledge of how the concentrations change over time, as well as knowing the dominating factor of the driving force and the rate of reduction at any point in time can be useful when deciding how to operate a furnace. If several identical experiments could be performed, and a stable set of parameters could be acquired, it might be possible to simulate similar experiments without having the experimental data beforehand. With that one could for example adjust the concentration of different additives to the charge to get the wanted slag and metal concentration.

5.2. K-values

To evaluate the validity of the model, the generated k-values can be compared to the average k-values calculated from experimental data by Olsø [22]. His values are shown in table 13, and are separated by varying slag chemistry represented by basicity and the ratio between Al_2O_3 and SiO_2, as well as the temperature. For comparison, the k-values generated by the model are shown in table 14. Here the values have been converted to (mg/min$\cdot$ cm^2), and the basicity and Al_2O_3/SiO_2 ratio has been calculated for each experiment. Using the activation energies, $E_{a,MnO}$ = 350,000 J/mol and E_{a,SiO_2} = 850,000 J/mol, the k-values were adjusted for temperature.

Table 13: Average k-values (mg/min· cm^2) from Olsø et al. [22]. Basicity and A/S are defined by the weight rations Basicity = $CaO/(SiO_2+Al_2O_3)$ and A/S = Al_2O_3/SiO_2 respectively.

		A/S=0.25	A/S=0.5
T (°C)	Basicity	k	k
1450	0.33	1.6	1.9
1450	0.67	1.4	1.2
1450	1	1.1	1
1500	0.33	4	3.8
1500	0.67	2.8	2.5
1500	1	2.3	2.1
1550	0.33	15.5	-
1550	0.67	9.5	-
1550	1	4.8	5

Table 14: Values for the rate constant k (mg/min· cm^2) from the model parameters. Basicity and A/S are defined by the weight rations Basicity = $(CaO+MgO)/(SiO_2+Al_2O_3)$ and A/S = Al_2O_3/SiO_2 respectively.

			kMn (mg/min cmˆ2)		
Experiment	Basicity	A/S	at 1450	at 1500	at 1550
Assmang 1	1.22	0.05	1.44	2.88	5.52
Assmang 2 curve fit	0.15	0.02	10.83	21.57	41.37
Assmang 2 value fit	0.34	0.16	29.48	58.72	112.60
Assmang 3	0.34	0.16	44.53	88.68	170.06
Holtan 1 slag fit	0.29	0.18	2.17	4.31	8.27
Holtan 1 metal fit	0.29	0.18	2.17	4.31	8.27
Holtan 2	0.30	0.18	3.01	5.99	11.49
Holtan 3	0.02	0.24	3.23	6.42	12.32
Skjervheim 70 metal fit	1.00	0.00	2.53	5.03	9.65
Skjervheim 70 slag fit	1.00	0.00	3.49	6.95	13.33
Skjervheim 72	0.43	0.40	1.32	2.64	5.06

Not taking into account the experiments where most foaming occured (Assmang 2 and 3), the values for k_0 are quite similar to the ones found by Olsø er al. The values found through the model are slightly higher, but the experiments also have a comparatively low basicity, and there seems to be a trend that a lower basicity yields a higher rate of reaction. This shows that the model provides results that concur with data found experimentally.

5.3. Experiment comparisons

Between the experiments done by Kim and Holtan, there is a difference in the ore used to make the charge. While Kim use Assmang ore, Holtan used Comilog, and though their experimental parameters were not exactly the same, the difference between the two experiment sets can still be studied. To compare these experiments, the rate constants and the temperatures of which foaming starts were studied, and three values were compared as a function of temperature, Mn content, Si content and rate of mass loss per square centimeter.

Table 15: The approximate temperature at which foaming or similar mechanics occurred during experiments.

Experiment	Foaming temperature
Assmang 2	1560 °C
Assmang 3	1520°C
Holtan 2	1550 °C
Holtan 3	1660 °C

Table 11 shows the rate constant of manganese and silicon reduction for each experiment. With the assumption that foaming is a part of the process and that the values found represent the average rate constant over the course of the experiment, it is very clear that Assmang ore reduces faster than Comilog ore. The rate constant for manganese is between 3 and 20 times as large for Assmang compared to Comilog, and while Comilog 2 has a higher rate for silicon, the remaining Comilog experiments are 10-100 times slower when it comes to silicon reduction as well.

The foaming temperature of each experiment in which foaming occured can be seen in table 15. The rapid increase of mass loss during Holtan 2 is considered foaming for this purpose, although no additional mass loss was observed during the experiment.

The foaming starts earlier on average in the Assmang experiments, but again Comilog 2 stands out and gives values closer to that of the Assmang experiments. The Assmang experiments also show a higher degree of mass loss as seen in table 12, with about 40% of the mass lost compared to around 15% in the Comilog experiments. This is a sign of higher gas production which would mean a faster reaction rate for Assmang compared to Comilog.

To study the temperature of which the manganese was reduced, a graph comparing the Mn content in the metal as a function of temperature was made. The graph can be seen in figure 30 and shows the mass percentage of Mn in the metal as a function of the temperature in °C for the Assmang and Comilog experiments.

From the graph in figure 30, it can be noted that Assmang 3 starts reducing MnO at a far lower temperature compared to the other experiments. This was the only experiment with HCFeMn included, and that was also the only difference from Assmang 2. This experiment also had the highest k_0, almost double that of Assmang 2 value fit, which leads to the conclusion that the inclution of HCFeMn increases the reactivity of MnO, and also makes it react at a lower temperature.

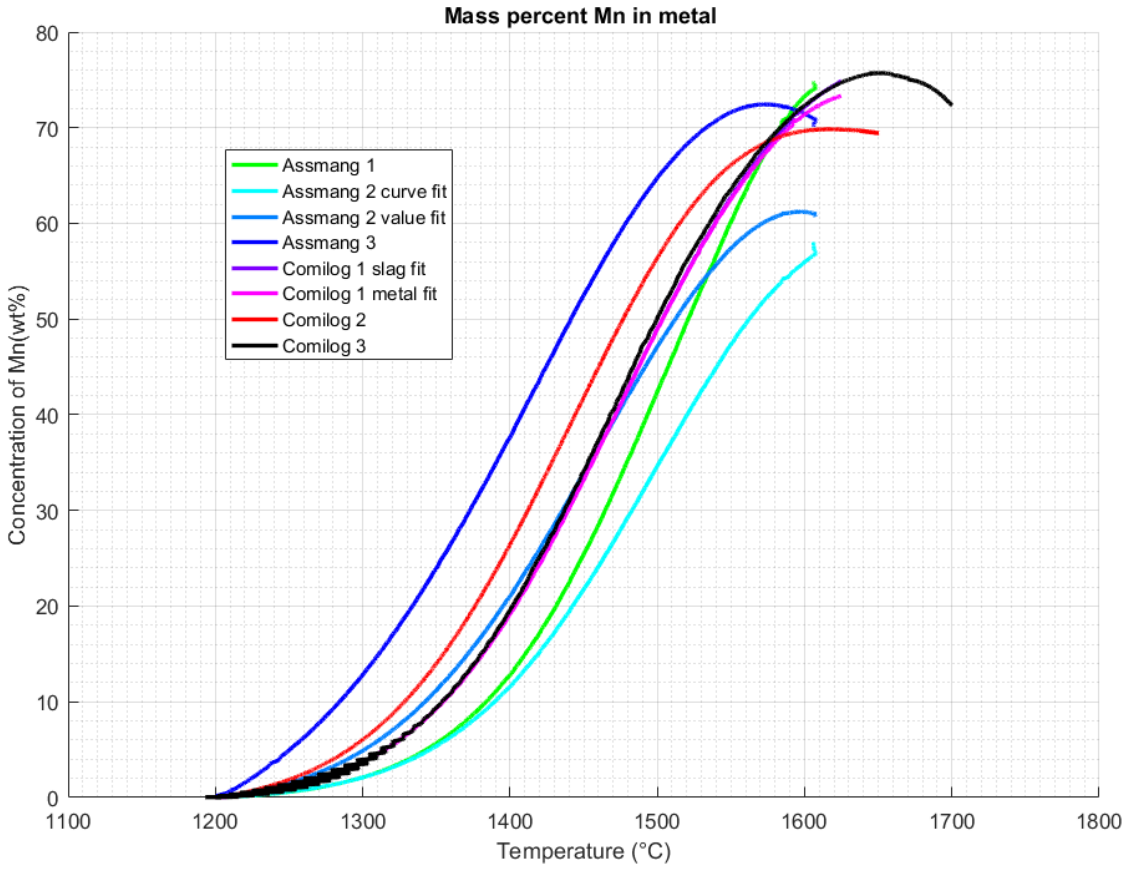

Figure 30: Mass percentage of Mn in the metal as a function of the temperature in °C for the Assmang and Comilog experiments.

To study the temperature of which the silicon was reduced, a graph comparing the Si content in the metal as a function of temperature was made. The graph can be seen in figure 31 and shows the mass percentage of Mn in the metal as a function of the temperature in °C for the Assmang and Comilog experiments.

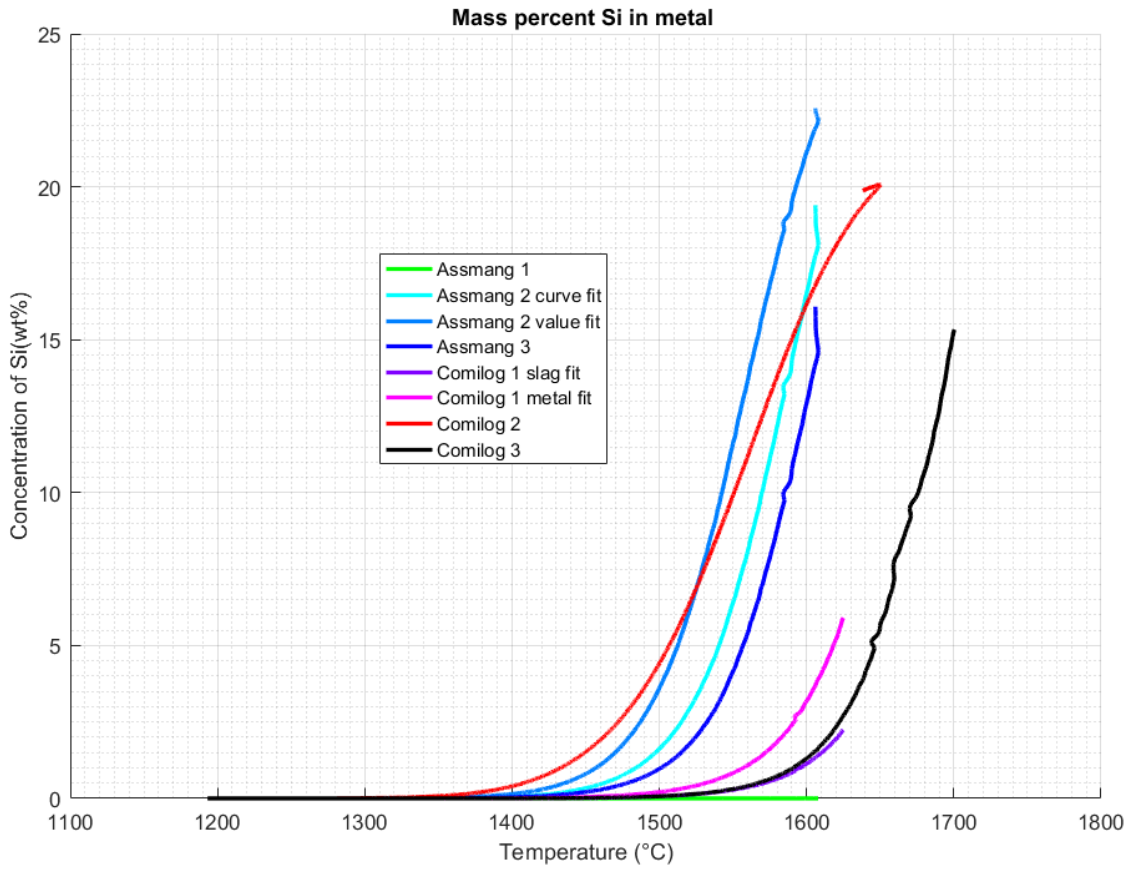

Figure 31: Mass percentage of Si in the metal as a function of the temperature in °C for the Assmang and Comilog experiments.

From the graph in figure 31, we can note that the Assmang experiments (excluding Assmang 1 as it did not have quartz) generally produced a higher Si content compared to the Comilog experiments, and also as lower temperatures. The exeption is Comilog 2, which is comparable to the Assmang experiments. This can also be seen through the k_0, Si values in table 11, where for Assmang 2 and 3 it is more than ten times larger than for Holtan 1 and 3, but less than half of Holtan 2. The only difference between Comilog 1 and 2 is the coke added on top, as well as the amount used as seen in table 7, but since the total mass is taken into account through the measuring of the reaction area, the added coke seems to be the reason for the difference. Discounting Holtan 2 however, the Assmang experiments has a faster SiO_2 reduction and ended with a higher Si content in the metal.

Lastly, a graph comparing the speed of weight loss as a function of temperature was made. The graph can be seen in figure 31 and shows the speed of weight loss divided by the reaction area as a function of the temperature in °C for the Assmang and Comilog experiments.

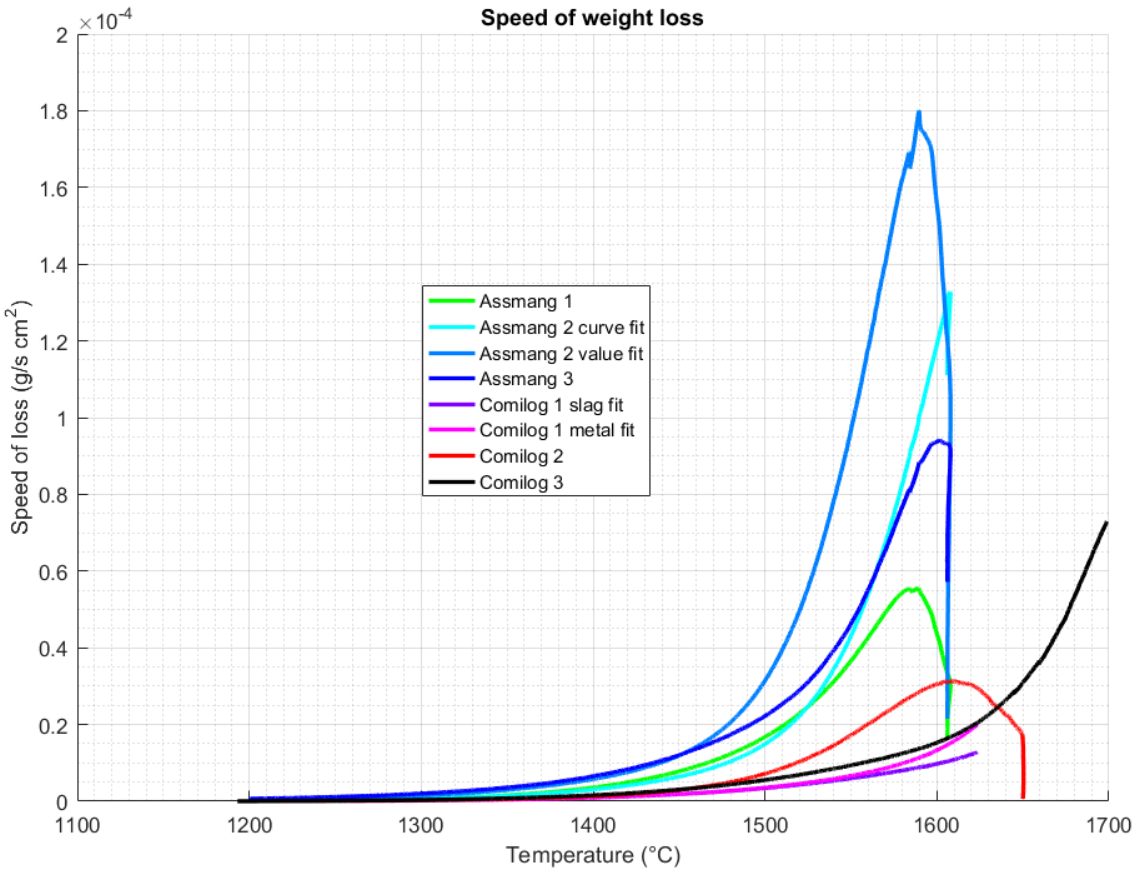

Figure 32: Speed of weight loss divided by reaction area as a function of the temperature in °C for the Assmang and Comilog experiments.

From the graph in figure 32, the difference in reaction rate between the Assmang and the Comilog experiments can be clearly seen. The mass loss rates for Assmang 1, 2 and 3 reaches their peak between 1575 and 1600 °C, and while Comilog 2 also reaches its peak at about the same temperature, the peak rate is just above half of that of the slowest Assmang experiment. It can be noted however, that the reaction rate for the Comilog experiments except Comilog 2 are all climbing. This points towards the conclusion that Comilog ore mostly just requires a higher temperature to react, and will if given the necessary heat react just as fast as Assmang ore.

5.4. Foaming and rapid mass loss

The graphs in figure 25 from experiment Comilog 2 shows how the reaction rate increases without losing mass. The peak rate from the experimental data is about five times the model's rate at the same point. Calculated coke/graphite reaction surface including extra coke is about 6.6 times larger than assumed reaction surface without the added coke. If the gas bubbling makes the slag wet almost all of the extra

coke, that would make the reaction rate fit almost perfectly.

For the rest of the experiments with foaming, the exact rate of weight loss is hard to establish, as some mass is lost through slag falling out of the furnace. The general tendency builds up under the theory that during foaming, the reaction area increases which leads to more powerful foaming untll the peak is reached and the MnO content goes towards equilibrium. It can be said from this that the foaming is a self-increasing process as it is triggered by the rate of gas production reaching a certain value, which is then further increased by the increase in reaction area.

5.5. Reasons for inaccuracy

As mentioned, there is a lack of precision in the model, primarily when attempts were made to fit it to several experiments using the same parameters. There are many possible reasons for this, and it is believed to be a sum of several of these that leads to the inaccuracy shown in the results. Following is a list of problems for which possible solutions will be proposed in section 6.1:

1) Differences in E_a: The activation energy of a reaction is not constant, and has been found to vary significantly for MnO in previous studies [14].

2) Inaccurate activity formulas: Both the slag and the metal are complicated systems for which accurate activity formulas are hard to make. The ones used in this project are considered accurate enough, but are by no means perfect.

3) Error in the data: The precision of measured data can never be 100% trusted, as error might come from both the instruments used and inhomogeneity where samples are taken.

4) Error in the model: It's likely that the model as it stands doesn't describe the complicated system of reactions well enough. This point can be split into several sub-points:

4.1) Wrong assumptions: Many assumptions were made, some which might have a larger impact than anticipated.

4.2) Missing factors: There might be other factors than the ones included in the model which influences the results.

5) Back diffusion might be present at an unknown rate. Some reactions might happen as the temperature lowers past the 1500 °C mark.

6. Conclusions and further work

- A theoretical study was done to create a model that could describe the reduction of both MnO and SiO_2. A formula for the reaction rate of the two most prominent reactions in the coke bed of the SiMn production process was suggested, and a list of variable parameters was created. Fitting was performed using Matlab R2016b to generate values for the parameters, which were compared and discussed.
- The model was shown to be able to simulate the experiments with a low degree of error. Although the foaming phenomenon was not duplicated, an averaged rate constant was found to provide the same degree of reduction. The model was capable of producing large amounts of data from the experiments, providing knowledge of what happens during the experiments.
- Assmang ore was found to show a higher rate of reduction for both MnO and SiO_2, and reacted at lower temperatures. This conclusion comes from the study of both foaming temperatures and rates, temperatures at and degrees of reduction of both Mn and Si, and the rate constants found. The study of the speed of weight loss for all experiments showed that Assmang reacted faster than Comilog in all cases.
- The temperature of which reduction started in experiment Assmang 3 was about 75°C lower compared to Assmang 2 as well as to the average of all the experiments. This is believed to be because of the addition of HCFeMn which was the only difference from experiment Assmang 2.

6.1. Possible solutions

A list of possible reasons for the inaccuracy of the model was proposed in section 5.2. Following is a list of proposed solution to these problems aimed towards improving the model:

1) Differences in E_a: The activation energy for a reaction can be measured using the Arrhenius equation [14], and by doing this for a large set of possible concentrations and temperatures, a general formula might be derivable.

2) Inaccurate activity formulas: Checking the values calculated by the formula towards a trusted source at different points could establish the degree of deviation. If too high, new formulas could be acquired and tested through the same method.

3) Error in the data: By studying a larger set of data, preferably several experiments for each set of conditions, this error can be minimized. Different weights can also be given to experimental data with varying degree of certainty.

4.1) Wrong assumptions: It might be possible to incorporate additional elements and/or formulas into the model instead of considering them to be negligible.

4.2) Too long time-steps: By reducing the length of each time-step, the balance equation might become applicable in all situations, as well as reducing error in general. This is the easiest solution to incorporate to the existing model, and should be considered including in any continuation of this project.

4.3) Missing factors: Additional factors can be added to attempt correction of errors related to

experiments with noticeable different factors such as charge particle size or impurity content.

7. Bibliography

[1] M. Tangstad. *The high carbon ferromanganese process - Coke bed relations*. PhD thesis, Norwegian Institute of Technology, 1996.

[2] S. E. Olsen, M. Tangstad, and T. Lindstad. *Production of manganese ferroalloys*. Tapir academic Press, Trondheim, 2007. ISBN 978-82-519-2191-6.

[3] T. Brynjulfsen. *Reduction of manganese ore agglomerates*. PhD thesis, Norwegian University of Science and Technology, 2013.

[4] E. Ringdalen, S. Gaal, M. Tangstad, and O. Ostrovski. Ore melting and reduction in silicomanganese production. *Metallurgical and materials transactions*, 41b:p1220–1229, December 2010.

[5] S. E. Olsen and M. Tangstad. Silicomanganese production process understanding. tenth international ferroalloys congress: INFACON X, February 2004. ISBN 0-9584663-5-1.

[6] P. Kim. PhD thesis, Norwegian University of Science and Technology, To be published.

[7] J. Holtan. Production of silicomanganese from comilog ore - reduction behaviour. Master's thesis, Norwegian University of Science and Technology, 2016.

[8] T. Skjervheim. *Kinetics and mechanisms for transfer of manganese and silicon molten oxide to liquid manganese metal*. PhD thesis, University of Trondheim, 1994.

[9] K. Terayama and M. Ikeda. Study on thermal decomposition of mno2 and mn2o, by thermal analysis. *Transactions of the Japan Institute of Metals*, 24, No. 11:p754–758, 1983.

[10] A. N. Grundy, B. Hallstedt, and L. J. Gauckler. Assessment of the mn-o system. *Journal of Phase Equilibria*, 24 no. 1:p21–39, 2003.

[11] K. T. Jacob, A. Kumar, G. Rajithal, and Y. Waseda. Thermodynamic data for mn3o4, mn2o3 and mno2. *High Temp. Mater. Proc.*, 30:p459–472, 2011.

[12] M. Tangstad and S. E. Olsen. The ferromanganese process - material and energy balance. *INFACON*, 7, June 1995.

[13] D. R. Swinbourne, W. J. Rankin, and E. H. Eric. The effect of alumina in slag on manganese and silicon distribution in silicomanganese smelting. *Metallurgical and materials transactions*, 26b:p59–65, February 1995.

[14] J. Safarian-Dastjerdi. *Kinetics and mechanisms of reduction of MnO-containing silicate slags by selected forms of carbonaceous materials*. PhD thesis, Norwegian University of Science and Technology, 2007.

[15] W. Ding and S. E. Olsen. Reaction equilibria in the production of manganese ferroalloys. *Metallurgical and materials transactions B*, 27B, February 1996.

[16] E. R. Cohen, T. Cvitas, J. G. Frey, B. Holmström, K. Kuchitsu, R. Marquardt, I. Mills,

F. Pavese, M. Quack, J. Stohner, H. L. Strauss, M. Takami, and A. J. Thor. *Quantities, units and symbols in physical chemistry*. IUPAC and RSC Publishing, Cambridge, 2008. ISBN 978-0-85404-433-7.

[17] P. Perrot. *A to Z of Thermodynamics*. Oxford University Press, Oxford, New York, and Tokyo, February 2000. ISBN 0-19-856556-9.

[18] A. Tanaka. The determination of the activities in mn-c and mn-si melts by the vapor pressure measurement. *Trans. JIM*, 20, 1979.

[19] A. Katsnelson, F. Tsukihashi, and N. Sano. Determination of manganeseand carbon activities of mn-c melts at 1628k. *ISIJ International*, 33, June 1993.

[20] Y. B. Kang, I. H. Jung, S. A. Decterov, A. D. Pelton, and H. G. Lee. Critical thermodynamic evaluation and optimization of the cao-mno-sio_2 and cao-mno-al_2o_3 systems. *ISIJ International*, 44 no. 6:p965–974, 2004.

[21] H. Ohta and H. Suito. Activities of sio_2 and al_2o_3 and activity coefficients of fe_to and mno in cao-sio_2-al_2o_3-mgo slags. *Metallurgical and materials transactions B*, 29B, February 1998.

[22] V. Ols, M. Tangstad, and S. E. Olsen. Reduction kinetics of mno-saturated slags. *INFACON*, 8:p259–283, June 1998.

[23] O. Ostrovski, S. E. Olsen, M. Tangstad, and M. Yastreboff. Kinetic modelling of mno reduction from manganese ore. *Canadian Metallurgical Quarterly*, 41-3:p309–318, March 2002.

[24] A. Blackman and L. Gahan. *Aylward and Findlay's SI Chemical Data, 7th Edition*. Wiley, New Jersey, 2014. ISBN 978-0-7303-0246-9.

[25] N. I. of Biomedical Imaging and Bioengineering. Computational modeling, July 2013. URL `https://www.nibib.nih.gov/sites/default/files/Computational%20Modeling%20Fact%20Sheet%20508.pdf`.